

# Massive Molecular Gas as a Fuel Tank for Active Galactic Nuclei Feedback in Central Cluster Galaxies

YUTAKA FUJITA,<sup>1</sup> NOZOMU KAWAKATU,<sup>2</sup> AND HIROSHI NAGAI<sup>3,4</sup>

<sup>1</sup>*Department of Physics, Graduate School of Science, Tokyo Metropolitan University,  
1-1 Minami-Osawa, Hachioji-shi, Tokyo 192-0397, Japan*

<sup>2</sup>*National Institute of Technology, Kure College,  
2-2-11, Agaminami, Kure, Hiroshima, 737-8506, Japan*

<sup>3</sup>*National Astronomical Observatory of Japan, Osawa 2-21-1, Mitaka, Tokyo 181-8588, Japan*

<sup>4</sup>*The Graduate University for Advanced Studies, SOKENDAI, Osawa 2-21-1, Mitaka, Tokyo 181-8588, Japan*

## ABSTRACT

Massive molecular gas has been discovered in giant elliptical galaxies at the centers of galaxy clusters. To reveal its role in active galactic nucleus (AGN) feedback in those galaxies, we construct a semianalytical model of gas circulation. This model especially focuses on the massive molecular gas (interstellar cold gas on a scale of  $\sim 10$  kpc) and the circumnuclear disk ( $\lesssim 0.5$  kpc). We consider the destruction of the interstellar cold gas by star formation and the gravitational instability for the circumnuclear disk. Our model can reproduce the basic properties of the interstellar cold gas and the circumnuclear disk, such as their masses. We also find that the circumnuclear disk tends to stay at the boundary between stable and unstable states. This works as an ‘adjusting valve’ that regulates mass accretion toward the supermassive black hole. On the other hand, the interstellar cold gas serves as a ‘fuel tank’ in the AGN feedback. Even if the cooling of the galactic hot gas is prevented, the interstellar cold gas can sustain the AGN activity for  $\gtrsim 0.5$  Gyr. We also confirm that the small entropy of the hot gas ( $\lesssim 30$  keV cm<sup>2</sup>) or the short cooling time ( $\lesssim 1$  Gyr) is a critical condition for the existence of the massive amounts of molecular gas in the galaxy. The dissipation time of the interstellar cold gas may be related to the critical cooling time. The galaxy behavior is described by a simple relation among the disk stability, the cloud dissipation time, and the gas cooling rate.

*Keywords:* Active galactic nuclei(16) — Brightest cluster galaxies(181) — Galaxy clusters(584) — Interstellar medium(847) — Molecular clouds(1072)

## 1. INTRODUCTION

Radiative cooling time of the hot intracluster medium (ICM) is often shorter than the Hubble time in the cores of many galaxy clusters. In the absence of any heating sources, the hot gas in the core should cool, and a ‘cooling flow’ toward the cluster center should develop (Fabian 1994). However, X-ray observations have denied the existence of massive cooling flows in clusters, indicating that the cores are heated by some unknown source (e.g. Ikebe et al. 1997; Kaastra et al. 2001; Peterson et al. 2001; Tamura et al. 2001). The active galactic nucleus (AGN) that resides in the central galaxy of a cluster is the most promising candidate of the heating source (AGN feedback; Churazov et al. 2000; McNamara & Nulsen 2007; Fabian 2012).

In addition to the hot X-ray gas, much cooler gas has been discovered in the central galaxies in the core of

galaxy clusters. For example, massive molecular clouds ( $\gtrsim 10^9 M_{\odot}$ ) have been detected, although the mass is much smaller than the prediction of a classical cooling flow model (Edge 2001; Salomé & Combes 2003; David et al. 2014; McNamara et al. 2014; Russell et al. 2014, 2016; Tremblay et al. 2016; Vantyghem et al. 2016). Nebular emission associated with warm gas has also been observed (Heckman et al. 1989; Crawford et al. 1999; McDonald et al. 2010; Tremblay et al. 2015). It has been indicated that the nebular emission, enhanced star formation, and AGN activity are tend to be observed in cluster cores when the central entropy drops down to  $\lesssim 30$  keV cm<sup>2</sup>, or almost equivalently when the central cooling time is  $\lesssim 1$  Gyr (Cavagnolo et al. 2008; Rafferty et al. 2008; Sanderson et al. 2009; Main et al. 2017).

While some of the molecular gas in the central galaxy is consumed in star formation, part of it may accrete onto the supermassive black hole (SMBH) at the galactic center. In fact, it has been discussed that the cold gas, rather than the hot gas, fuels the SMBH (Shlosman et al. 1989; Pizzolato & Soker 2010). However, the angular momentum would hinder the radial infall of the gas, which leads to the formation of a circumnuclear disk around the SMBH ( $\lesssim 0.5$  kpc). Active star formation has been observed in the circumnuclear disk as nuclear starbursts in nearby galaxies (Imanishi & Wada 2004; Davies et al. 2007; Watabe et al. 2008). Previous studies have indicated that the star formation can induce the mass accretion onto the SMBH (e.g. Umemura et al. 1997; Wada & Norman 2002; Thompson et al. 2005; Levin 2007; Vollmer et al. 2008; Kumar & Johnson 2010). In particular, the turbulence generated by supernova (SN) explosions associated with the star formation may regulate the kinetic viscosity of the disk and may change the mass accretion rate (Kawakatu & Wada 2008; Wutschik et al. 2013). This means that the tiny circumnuclear disk may control AGN feedback and may affect the evolution of the central galaxy and the cluster core.

In this paper, we study AGN feedback and gas circulation of the central galaxies in cluster cores using a semianalytical model. We employ a semianalytical model because although a number of numerical simulations have been performed for the formation of cold gas and the AGN feedback (e.g. Ciotti & Ostriker 2007; Ciotti et al. 2010; Barai et al. 2012; McCourt et al. 2012; Sharma et al. 2012; Gaspari et al. 2013; Hardcastle & Krause 2013; Guo & Mathews 2014; Meece et al. 2015; Bourne & Sijacki 2017; Ciotti et al. 2017; Weinberger et al. 2017; Bourne et al. 2019; Qiu et al. 2019a,b, 2020; Yao et al. 2021), it is still difficult to cover the whole scale from the cluster core ( $\sim 30$  kpc) to the star formation and turbulence in the circumnuclear disk ( $\lesssim$  pc). Moreover, it is much easier to interpret the results of semianalytical models than those of numerical simulations. In this study, we focus on the roles of the massive molecular gas and the circumnuclear disk in the AGN feedback. We construct our model based on representative models of molecular gas evolution (Elmegreen & Efremov 1997) and the circumnuclear disk (Kawakatu & Wada 2008; Wutschik et al. 2013). This paper is organized as follows. In Section 2, we describe our models for the gas circulation and the AGN feedback. In Section 3, we indicate that the resulting behavior of the model galaxy can be represented by a simple relation. In Section 4, we show the results of our fiducial model. In Section 5, we discuss the roles of the massive molec-

ular gas clouds and the circumnuclear disk in the AGN feedback as well as the influence of the entropy of the hot gas. The conclusion of this paper is presented in Section 6.

## 2. MODELS

### 2.1. Overview

Figure 1 shows a flow chart of the relations among different gas components. Although we later construct evolution equations following this chart (see Section 2.6), here we briefly explain the whole picture of gas flows among the components. The 'hot gas' in the galaxy cools through radiative cooling and becomes the 'interstellar cold gas', which corresponds to the observed massive molecular gas ( $\gtrsim 10^9 M_\odot$  see Section 1). Thus, the mass of the interstellar cold gas ( $M_{g,i}$ ) depends on the supply from the hot gas ( $\dot{M}_{cool}$ ). While most of the interstellar cold gas turns into galactic stars with a disruption time-scale  $t_{dis,c}$  and a star formation efficiency  $\epsilon_{*,c}$  (arrow (a) in Figure 1), the rest eventually flows into the galactic center at a rate of  $\dot{M}_{sup}$  and forms the 'circumnuclear disk' around the SMBH. The mass of the disk is represented by  $M_{g,d}$  and it is typically  $\sim 10^8 M_\odot$  (Nagai et al. 2019). Because the circumnuclear disk can also contain molecular gas, we use the term 'interstellar cold gas' instead of molecular gas. Some of the disk gas pours into the SMBH at a rate of  $\dot{M}_{BH}$  and the rest is consumed in star formation in the disk with an efficiency of  $C_*$  (arrow (c) in Figure 1). The gas attracted by the SMBH activates the AGN, which prevents the galactic hot gas from cooling further (dashed-arrow in Figure 1). The energy injection rate of the AGN is represented by  $L_{AGN}$ . The masses of the galactic and the disk stars are represented by  $M_{*,i}$  and  $M_{*,d}$ , respectively. Some fraction ( $R_{ret}$ ) of the stellar mass goes back to the hot gas (arrows (b) and (d) in Figure 1). In the following subsections, we describe the details of each component. The list of main parameters is shown in Table 1.

### 2.2. Galaxy potential

We assume that the central galaxy and the host cluster are spherically symmetric except for the circumnuclear disk, and that the SMBH is located at  $r = 0$ . The gravitational potential around the galaxy is mainly composed of two components (Hogan et al. 2017a; Pulido et al. 2018). One is a central-core isothermal potential representing the galaxy,

$$\Phi_{ISO}(r) = -\sigma^2 \ln(1 + (r/r_I)^2), \quad (1)$$

where  $\sigma$  is the stellar velocity dispersion, and  $r_I$  is the core radius. The other is a Navarro-Frenk-White

**Table 1.** List of main parameters and symbols

Parameter	Symbol	Equations or sections
(1)	(2)	(3)
Potential of the galaxy component	$\Phi_{\text{ISO}}$	(1)
Potential of the cluster component	$\Phi_{\text{NFW}}$	(2)
Potential of newly formed stars	$\Phi_{\text{nstar}}$	(3)
Total potential	$\Phi$	(3)
Total mass	$M_{\text{host}}$	2.2
Galaxy radius	$r_{\text{gal}}$	2.3
Density of the hot gas	$\rho_{\text{hot}}$	(4)
$\rho_{\text{hot}}$ at $r_{\text{gal}}$	$\rho_{\text{hot},0}$	(4)
Mass of the hot gas	$M_{\text{hot}}$	(5)
Virial temperature of the galaxy	$kT_{\text{vir}}$	(6)
Average hot gas temperature	$kT_{\text{hot}}$	(7)
Cooling function of the hot gas	$\Lambda$	(8)
X-ray luminosity of the galaxy	$L_{\text{cool}}$	(9)
Effective cooling radius	$r_{\text{cool}}$	(9)
Electron number density	$n_e$	(9)
$n_e$ at $r_{\text{gal}}$	$n_{e,0}$	2.3
Cooling rate of the hot gas	$\dot{M}_{\text{cool}}$	(10)
Unsuppressed $\dot{M}_{\text{cool}}$	$\dot{M}_{\text{cool},0}$	(11)
Mass of a molecular cloud	$M_c$	(12)
Mass of stars in a cloud	$M_{*,c}$	(12)
Luminosity of stars in a cloud	$L_{*,c}$	(12)
Turbulent velocity of cloud gas	$v_{t,c}$	2.4.1
Cloud disruption time	$t_{\text{dis},c}$	(13)
Efficiency of star formation	$\epsilon_{*,c}$	(13)
Mass of the interstellar cold gas	$M_{g,i}$	2.4.1
Extent of the interstellar cold gas	$r_i$	2.4.2
Cooling time of the hot gas	$t_{\text{cool}}$	2.4.2
Free-fall time	$t_{\text{ff}}$	2.4.2
Gravity of the galaxy	$g$	2.4.2
Mass of the SMBH	$M_{\text{BH}}$	(14)
Disk gas mass	$M_{g,d}$	(14)
Disk radius	$r_d$	(14)
Critical surface density of the disk	$\Sigma_{\text{crit}}$	(15)
Sound velocity of the disk gas	$c_{s,d}$	(15)
Angular velocity of the disk	$\Omega$	(16)
Disk gas density	$\rho_d$	(17)
Turbulent velocity of the disk gas	$v_{t,d}$	(17)
Scale height of the disk	$h$	(17),(22),(23)
Surface density of the disk	$\Sigma_d$	(18)
Vertical gravity of the disk	$g_d$	(18)
Heating efficiency of SNe	$\eta$	(19)
Star formation rate of the disk	$S_*$	(19)
SN energy	$E_{\text{SN}}$	(19)
Dissipation time of disk turbulence	$t_{\text{dis},d}$	(19)
Star formation efficiency of the disk	$C_*$	(20)
SMBH accretion rate	$\dot{M}_{\text{BH}}$	(24)
Coefficient of disk viscosity	$\nu$	(24),(25),(26)
$\alpha$ -parameter of the disk	$\alpha$	(25),(26)
AGN power	$L_{\text{AGN}}$	(27)
Heating efficiency of the AGN	$\epsilon_{\text{heat}}$	(27)
Cooling suppression factor	$f_{\text{sup}}$	(28)
Supply from the cold interstellar gas	$\dot{M}_{\text{sup}}$	(31)
Return fraction of the stellar mass	$R_{\text{ret}}$	(32)
Stellar mass in the interstellar cold gas	$M_{*,i}$	(32)
Stellar mass in the disk	$M_{*,d}$	(33)
Specific entropy	$K$	5.2
Specific entropy at $r = 30$ kpc	$K_{30}$	5.2
Star formation rate of the galaxy	$\dot{M}_*$	(37)

NOTE—The representative equations or sections in which the parameters appear are shown in the column (3).

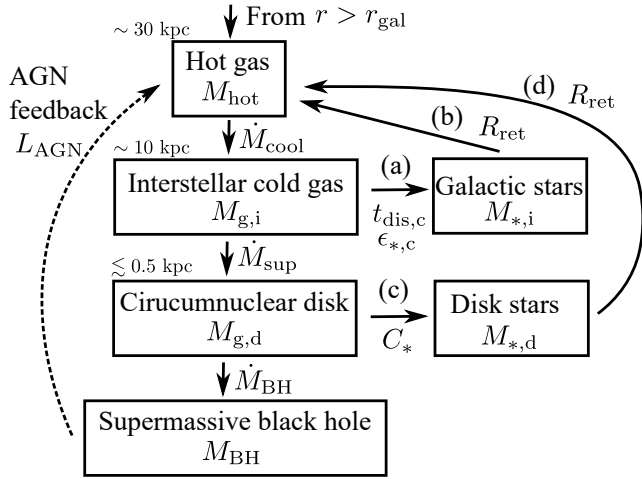


**Figure 1.** Flow chart showing the different components in the galaxy. The solid arrows show gas flows, and the dotted arrow shows the AGN feedback. The spacial scales of the hot gas, the interstellar cold gas, and the circumnuclear disk are presented.

(NFW) potential of the host cluster,

$$\Phi_{\text{NFW}}(r) = -4\pi G \rho_0 r_s^2 \frac{\ln(1 + r/r_s)}{r/r_s}, \quad (2)$$

where  $\rho_0$  is the characteristic matter density, and  $r_s$  is the scale radius (Navarro et al. 1997). In this paper, we assume that  $\sigma = 250 \text{ km s}^{-1}$ ,  $r_s = 400 \text{ kpc}$ , and  $4\pi G \rho_0 r_s^2 \mu m_p = 40 \text{ keV}$ , where  $\mu = 0.6$  is the mean molecular weight, and  $m_p$  is the proton mass. These values are typical ones for clusters and the central galaxies (Hogan et al. 2017a; Pulido et al. 2018). For the core radius of the galaxy, we adopt  $r_{\text{I}} = 0.8 \text{ kpc}$  (e.g. Wilman et al. 2005; Okabe et al. 2016). We also consider the gravitational potential associated with newly formed stars in the interstellar cold gas and the circumnuclear disk,  $\Phi_{\text{nstar}}(r)$ , which will be given in section 2.6. The contribution of gas to the potential is ignored. Thus, the potential of the whole system is represented by

$$\Phi(r) = \Phi_{\text{ISO}}(r) + \Phi_{\text{NFW}}(r) + \Phi_{\text{nstar}}(r), \quad (3)$$

and the mass distribution corresponding to  $\Phi(r)$  is referred to as  $M_{\text{host}}(r)$ .

### 2.3. Hot gas

We focus on gas circulation and AGN feedback in the innermost region of a cluster, that is, within the central galaxy. We define the influential sphere of the central galaxy as  $r < r_{\text{gal}}$ , and we adopt  $r_{\text{gal}} = 30 \text{ kpc}$  as the ‘boundary’. The region  $r < r_{\text{gal}}$  generally covers the stellar system of the galaxy (Okabe et al. 2016). Since our main interest is the interstellar cold gas and the

circumnuclear disk, we adopt a simplified model for the hot gas. Thus, we assume that the gas density at the boundary  $r = r_{\text{gal}}$  is constant, and the density profile is given by a power law

$$\rho_{\text{hot}}(r) = \rho_{\text{hot},0} (r/r_{\text{gal}})^{-\alpha_{\text{hot}}}. \quad (4)$$

Moreover, in order to avoid complexity, we assume that  $\alpha_{\text{hot}}$  is time-independent, which means that the mass of the hot gas for  $r < r_{\text{gal}}$  is constant. This implies that, if some of the hot gas is removed through radiative cooling, the equal amount of hot gas is supplied from the outside of the boundary ( $r > r_{\text{gal}}$ ). While this may rather be an oversimplification, it allows us to study the influence of boundary conditions at  $r = r_{\text{gal}}$  on the results. In our fiducial model, we assume that the electron density at  $r = r_{\text{gal}}$  is  $n_{\text{e},0} = 0.86 \rho_{\text{hot},0}/m_p = 0.02 \text{ cm}^{-3}$  and that the index is  $\alpha_{\text{hot}} = 1$  (Equation (4)). Those are typical values for cool-core clusters (Hogan et al. 2017a). The mass of the hot gas is

$$M_{\text{hot}}(r) = 4\pi \int_0^r \rho_{\text{hot}}(r) r^2 dr. \quad (5)$$

The temperature of the hot gas basically reflects the virial temperature of the galaxy, which is given by

$$kT_{\text{vir}} = |\Phi(r_{\text{gal}})|/2, \quad (6)$$

where  $k$  is the Boltzmann constant. Observations have shown that the temperature of the hot gas around the central galaxies of clusters is a factor of 2 larger than the virial temperature (Matsushita 2001; Nagino & Matsushita 2009). Thus, the hot gas temperature  $kT_{\text{hot}}$  is given by

$$kT_{\text{hot}} = 2 kT_{\text{vir}} \quad (7)$$

For the parameters we selected in Section 2.2,  $kT_{\text{hot}} \sim 2.2 \text{ keV}$ .

The hot gas loses its thermal energy through radiative cooling. For the cooling function, we adopt the following metallicity-dependent one:

$$\begin{aligned} \Lambda(T, Z) = & 2.41 \times 10^{-27} \left[ 0.8 + 0.1 \left( \frac{Z}{Z_{\odot}} \right) \right] \left( \frac{T}{\text{K}} \right)^{0.5} \\ & + 1.39 \times 10^{-16} \left[ 0.02 + \left( \frac{Z}{Z_{\odot}} \right)^{0.8} \right] \\ & \times \left( \frac{T}{\text{K}} \right)^{-1.0} \text{ erg cm}^3 \text{ s}^{-1} \end{aligned} \quad (8)$$

(Fujita & Ohira 2013), where  $T$  is the temperature, and  $Z$  is the metallicity. This function approximates the one derived by Sutherland & Dopita (1993) for  $T \gtrsim 10^5 \text{ K}$  and  $Z \lesssim 1 Z_{\odot}$ . Since we consider the hot gas inside the central galaxy, we assume that  $Z = 0.5 Z_{\odot}$ .

The X-ray luminosity of the galaxy is given by

$$L_{\text{cool}} = \int_0^{r_{\text{cool}}} 4\pi r^2 n_e(r)^2 \Lambda(T_{\text{hot}}, Z) dr, \quad (9)$$

where  $n_e(r)$  is the electron number density, and it is given by  $n_e = 0.86 \rho_{\text{hot}}/m_p$ . The upper limit of the integral  $r_{\text{cool}}$  is the radius within which radiative cooling is effective, which will be specified in Section 2.4.2. The cooling rate of the hot gas is written as

$$\dot{M}_{\text{cool}} = \dot{M}_{\text{cool},0} f_{\text{sup}}, \quad (10)$$

where

$$\dot{M}_{\text{cool},0} = \frac{2}{5} \frac{\mu m_p L_{\text{cool}}}{k T_{\text{hot}}} \quad (11)$$

(e.g. Fabian 1994), and  $f_{\text{sup}}$  is the suppression factor by AGN feedback, which will be given in Equation (28).

## 2.4. Interstellar cold gas cloud

### 2.4.1. Evolution

The evolution of the interstellar cold gas is affected by the surrounding pressure and the star formation in the cold gas. We treat the gas as a massive cold cloud and adopt the model by Elmegreen & Efremov (1997), although it is not obvious whether this model, which was constructed for Milky Way clouds, can be applied to the filamentary cold gas observed in cluster cores.

In the model by Elmegreen & Efremov (1997), the cloud mass  $M_c$  evolves as

$$\frac{dM_c}{dt_c} = -\frac{dM_{*,c}}{dt_c} - \frac{AL_{*,c}}{v_{t,c}^2}, \quad (12)$$

where  $t_c$  is the time lapsed since the cloud is formed,  $M_{*,c}$  is the mass of the stars that are formed in the cloud,  $L_{*,c}$  is the luminosity of the stars,  $v_{t,c}$  is the turbulent velocity of the cloud gas, and  $A$  is a dimensionless constant. The binding energy of the cloud is written as  $M_c v_{t,c}^2$ , and the turbulent velocity is given by  $v_{t,c} \propto (P_c M_c^2)^{1/8}$ , where  $P_c$  is the cloud pressure (Elmegreen 1989). The star formation rate  $dM_{*,c}/dt_c$  is assumed to be constant.

The cloud disruption time  $t_{\text{dis},c}$  is defined as the time when the cloud mass reaches zero ( $M_c = 0$ ). The efficiency of star formation  $\epsilon_{*,c}$  is given by

$$\epsilon_{*,c} = \frac{dM_{*,c}}{dt_c} \frac{t_{\text{dis},c}}{M_c(t_c = 0)}. \quad (13)$$

Both  $t_{\text{dis},c}$  and  $\epsilon_{*,c}$  can be derived analytically as functions of  $P_c$  and  $M_c(t_i = 0)$  and we show the results in Figure 2 for  $P_c = 100 P_\odot$ , where  $P_\odot = 3 \times 10^4 \text{ cm}^{-3} \text{ K}$  is the pressure in the solar neighborhood. The disruption time  $t_{\text{dis},c}$  is an increasing function of  $M_c$  because

it is proportional to the crossing time of a molecular cloud  $R_c/v_{t,c}$ , where  $R_c$  is the cloud radius (Elmegreen & Efremov 1997). Moreover, the efficiency of star formation  $\epsilon_{*,c}$  is also an increasing function of  $M_c$  because it depends on the binding energy of the cloud (Elmegreen & Efremov 1997).

In this study, we adopt  $t_{\text{dis},c}$  and  $\epsilon_{*,c}$  for  $P_c = 100 P_\odot$  (Figure 2). The adopted value of  $P_c$  is roughly consistent with the assumed hot gas pressure of our model galaxy (Equations (4) and (7)), and  $t_{\text{dis},c}$  and  $\epsilon_{*,c}$  are not much sensitive to  $P_c$ . Since  $P_c$  is fixed, the disruption time and the efficiency can be represented by  $t_{\text{dis},c} = t_{\text{dis},c}(M_c)$  and  $\epsilon_{*,c} = \epsilon_{*,c}(M_c)$ , respectively. Compared to those for the solar neighborhood ( $P = P_\odot$ ),  $t_{\text{dis},c}$  is smaller and  $\epsilon_{*,c}$  is larger at  $P_c = 100 P_\odot$  for a given  $M_c$  (see Figure 4 in Elmegreen & Efremov 1997).

The above model describes the evolution of a cold cloud without an additional mass supply. For the central galaxy we consider, however, we need to include the mass supply from hot gas  $\dot{M}_{\text{cool}}$  (Equation (10) and Figure 1), which means that the evolution of the cold interstellar gas does not simply follow Equation (12). Thus, when we consider the evolution of the interstellar cold gas in Section 2.6, we use the letter  $M_{g,i}$  instead of  $M_c$  in order to clarify the difference, and we use the values  $t_{\text{dis},c}(M_{g,i})$  and  $\epsilon_{*,c}(M_{g,i})$  as variable parameters in evolution Equations (29)–(32). These two parameters determine the evolution of the interstellar cold gas.

### 2.4.2. Spatial distribution

Observationally, the cold interstellar gas has been detected in the region where the cooling time of the hot gas is  $t_{\text{cool}} \lesssim 1 \text{ Gyr}$  (e.g. Pulido et al. 2018; Russell et al. 2019). This suggests that strong thermal instability develops when  $t_{\text{cool}} \lesssim 1 \text{ Gyr}$  (Cavagnolo et al. 2008; Rafferty et al. 2008; Mittal et al. 2009; Hudson et al. 2010; Main et al. 2017). In this study, we define the threshold radius  $r_i$  as the one where the cooling time is  $t_{\text{cool}} = 0.7 \text{ Gyr}$ , which is the typical value observed for cool-core clusters (Pulido et al. 2018; Russell et al. 2019). We assume that the cold interstellar gas is distributed at  $r < r_i$ . On the other hand, the hot gas loses its thermal energy even at  $r > r_i$  and we assume that the cooling is effective up to  $r_{\text{cool}} = f_{\text{cool}} r_i$ , where  $f_{\text{cool}}$  is a constant. Observations have shown that optical filaments, which are apparently formed through radiative cooling, surround molecular gas at the center of clusters. The size of the optical filaments is  $\sim 4$  times larger than that of molecular gas (e.g. Olivares et al. 2019). Thus, we adopt  $f_{\text{cool}} = 4$  in this study.

Previous studies have indicated that the thermal instability develops in the hot gas when  $t_{\text{cool}}/t_{\text{ff}} \lesssim 20$ ,



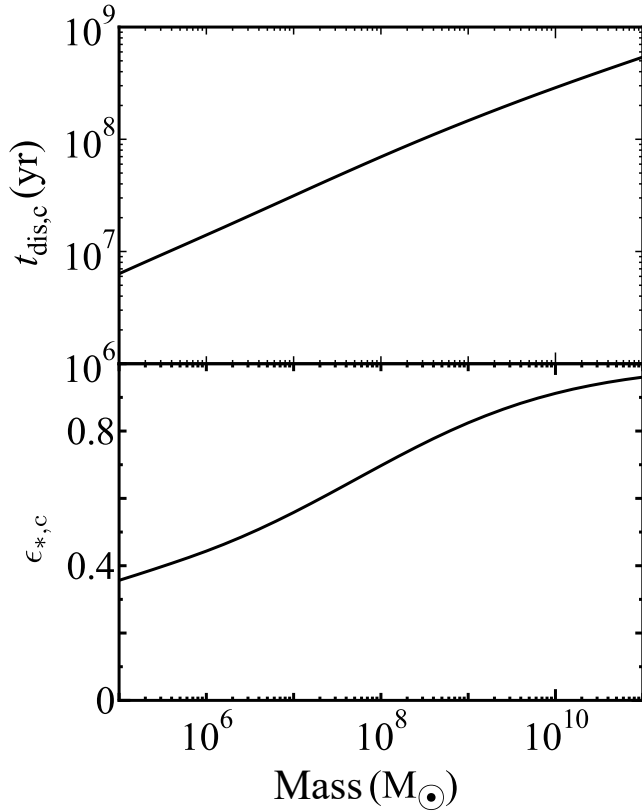


**Figure 2.** Disruption time  $t_{\text{dis},c}$  (upper) and  $\epsilon_{*,c}$  (lower) represented as functions of the cloud mass when  $P_c = 100P_\odot$ .

where  $t_{\text{ff}} = \sqrt{2r/g}$  is the free-fall time, and  $g$  is the gravitational acceleration (Gaspari et al. 2012; McCourt et al. 2012; Li et al. 2015; Prasad et al. 2015; Voit & Donahue 2015; Voit et al. 2015, 2017; McNamara et al. 2016). In our fiducial model,  $t_{\text{cool}}/t_{\text{ff}} \sim 20$  at  $r = r_i \sim 11$  kpc, which means that the thermal instability should develop.

## 2.5. Circumnuclear disk and AGN feedback

### 2.5.1. Disk radius and stability

The gas of the circumnuclear disk is supplied from the interstellar cold gas. We assume that the interstellar cold gas that is not consumed in star formation eventually gathers at the galaxy center and forms the circumnuclear disk, even if the gas has been warmed up by the stars. This is because the interstellar cold gas is deposited from the hot gas that is in hydrostatic equilibrium, which may mean that the cold gas has little angular momentum. Thus, the cold gas that does not form stars should almost radially fall toward the galactic center, and the circumnuclear disk is formed through the residual angular momentum.

We construct a model of the disk based on those developed by Kawakatu & Wada (2008) and Wutschik et al. (2013). For the sake of simplicity, we do not consider the

radial structure of the disk in contrast with those previous studies. Thus, the disk is represented as a one-zone system in this study.

For the sake of simplicity, we assume that the disk radius  $r_d$  is the farthest reach of the dominion of the gravitational potential of the disk with respect to the host galaxy (Wutschik et al. 2013). Thus, it can be derived by numerically solving equation of

$$M_{\text{BH}} + M_{\text{g,d}} = M_{\text{host}}(r_d), \quad (14)$$

where  $M_{\text{BH}}$  is the mass of the SMBH and  $M_{\text{g,d}}$  is the gas mass of the disk, which is given by solving Equation (30). In the fiducial model, the disk size is  $r_d \sim 0.4$  kpc.

The disk has two states: (i) a gravitationally unstable state and (ii) a gravitationally stable state. We adopt Toomre's stability criterion to distinguish them (Toomre 1964; see also Romeo & Falstad 2013). The critical surface density is defined as

$$\Sigma_{\text{crit}} = \frac{\kappa c_{\text{s,d}}}{\pi G}, \quad (15)$$

where  $\kappa^2 = 4\Omega(r_d)^2 + 2\Omega(r_d)r_d\Omega/dr$  is the epicyclic frequency, and  $c_{\text{s,d}}$  is the sound velocity of the disk gas. We assume that  $c_{\text{s,d}} = 1$  km s $^{-1}$  following Kawakatu & Wada (2008). The angular velocity  $\Omega(r)$  is given by

$$\Omega(r)^2 = \frac{G(M_{\text{BH}} + M_{\text{host}}(r))}{r^3} + \frac{\pi G \Sigma_d}{r}. \quad (16)$$

The surface density of the disk is represented by  $\Sigma_d = M_{\text{g,d}}/(\pi r_d^2)$ . The stability criterion indicates that if  $\Sigma_d > \Sigma_{\text{crit}}$  ( $\Sigma_d < \Sigma_{\text{crit}}$ ), the disk is unstable (stable). This corresponds to  $Q < 1$  (unstable) and  $Q > 1$  (stable) in terms of the Toomre  $Q$  parameter.

### 2.5.2. Unstable disk

When the disk is unstable ( $\Sigma_d > \Sigma_{\text{crit}}$ ), star formation is triggered, and the disk is supported by the turbulent pressure associated with supernovae (SNe) explosions in the disk. Thus, the pressure is given by  $\rho_d v_{\text{t,d}}^2$ , where  $\rho_d$  is the disk gas density, and  $v_{\text{t,d}}$  is the turbulent velocity. The pressure is balanced with the vertical gravity of the disk  $g_d$ :

$$\rho_d v_{\text{t,d}}^2 = \rho_d g_d h, \quad (17)$$

where  $h$  is the scale height of the disk. The surface density of the disk is also represented as  $\Sigma_d = 2\rho_d h$ . The gravity component perpendicular to the disk is

$$g_d = \frac{G(M_{\text{BH}} + M_{\text{host}}(r_d))h}{r_d^3} + \pi G \Sigma_d. \quad (18)$$

Since the turbulence is driven by SN explosions, the energy balance can be expressed as

$$\frac{\rho_d v_{\text{t,d}}^2}{t_{\text{dis,d}}} = \eta S_* E_{\text{SN}} \quad (19)$$

where  $\eta$  is the heating efficiency,  $S_*$  is the star formation rate per unit volume and time, and  $E_{\text{SN}} (= 10^{51} \text{ erg})$  is the energy input by a SN explosion. Since the dissipation time of the turbulence is given by  $t_{\text{dis,d}} = h/v_{\text{t,d}}$  and the star formation rate is represented by  $S_* = C_* \rho_{\text{d}}$ , where  $C_*$  is the star formation efficiency, Equation (19) can be rewritten as

$$\frac{v_{\text{t,d}}^3}{h} = \eta C_* E_{\text{SN}} \quad (20)$$

From Equations (17), (18), (20), one can obtain

$$h^{1/2} \left[ \frac{G(M_{\text{BH}} + M_{\text{host}}(r_{\text{d}}))h}{r_{\text{d}}^3} + \pi G \Sigma_{\text{d}} \right]^{3/2} = \eta C_* E_{\text{SN}} \quad (21)$$

The disk height  $h$  can be derived by numerically solving this equation, and then the turbulent velocity  $v_{\text{t,d}}$  can be obtained from Equation (20). We assume that  $\eta = 10^{-3} M_{\odot}^{-1}$  and  $C_* = 3 \times 10^{-8} \text{ yr}^{-1}$ , following Kawakatu & Wada (2008). We note that this disk model (see also Kawakatu et al. 2020) is supported by recent observations. For example, Nagai & Kawakatu (2021) detected diffuse synchrotron emission that is associated with star formation in the circumnuclear disk of NGC 1275. They also indicated the turbulent velocity of the circumnuclear disk observed with the Atacama Large Millimeter/submillimeter Array (ALMA) is consistent with the model. Moreover, the correlation between the mass of dense molecular gas around the galactic centers and the SMBH mass accretion rate may also support the disk model (Izumi et al. 2016).

### 2.5.3. Stable disk

When the disk is stable ( $\Sigma_{\text{d}} < \Sigma_{\text{crit}}$ ), the disk is supported by thermal pressure  $\rho_{\text{d}} c_{\text{s,d}}^2$ , which is balanced with the vertical gravity of the disk:

$$\rho_{\text{d}} c_{\text{s,d}}^2 = \rho_{\text{d}} g_{\text{d}} h. \quad (22)$$

Thus, the disk height is given by

$$h = \frac{c_{\text{s,d}}^2}{g_{\text{d}}}. \quad (23)$$

We assume that the star formation in the disk ceases ( $C_* = 0$ ) during the stable state.

### 2.5.4. Mass accretion toward SMBH and AGN feedback

We suppose that kinetic viscosity is the cause of angular momentum transfer in the gas disk. In this case, the mass accretion rate toward the SMBH is given by

$$\dot{M}_{\text{BH}} = 2\pi\nu\Sigma_{\text{d}} \left| \frac{d \ln \Omega(r_{\text{d}})}{d \ln r_{\text{d}}} \right|, \quad (24)$$

where  $\nu$  is the coefficient of kinetic viscosity (Pringle 1981).

The coefficient  $\nu$  depends on the state of the disk. When the disk is unstable ( $\Sigma_{\text{d}} > \Sigma_{\text{crit}}$ ), the coefficient is

$$\nu = \alpha v_{\text{t,d}} h, \quad (25)$$

where  $\alpha$  is the so-called  $\alpha$ -parameter. Following Kawakatu & Wada (2008), we adopt  $\alpha = 1$ , which is based on numerical simulations (Wada & Norman 2002). On the other hand, when the disk is stable ( $\Sigma_{\text{d}} < \Sigma_{\text{crit}}$ ), the coefficient is

$$\nu = \alpha c_{\text{s,d}} h. \quad (26)$$

In this case, the magnetorotational instability could be a source of turbulence. The turbulent velocity is comparable to or even smaller than the sound velocity, and the  $\alpha$ -parameter is represented by  $\alpha \sim 0.01\text{--}0.5$  (e.g. Balbus & Hawley 1991; Machida et al. 2000; Machida & Matsumoto 2003). In this study, we adopt  $\alpha = 0.05$ .

The potential energy of the gas accreted by the SMBH is converted to radiation, winds or jets, which could heat the galaxy (AGN feedback). The energy input rate by the AGN is

$$L_{\text{AGN}} = \epsilon_{\text{heat}} \dot{M}_{\text{BH}} c^2, \quad (27)$$

where  $\epsilon_{\text{heat}}$  is the heating efficiency, and we adopt  $\epsilon_{\text{heat}} = 0.02$  (Lacey et al. 2016). We assume that the AGN feedback acts only on the hot gas, because the volume filling factor of the interstellar cold gas and circumnuclear gas is very small. If AGN feedback is effective, it should prevent the hot gas from cooling. Since the actual feedback mechanism has not been well understood and it may be quite complicated, such as sound waves (Fabian et al. 2006, 2017; Zweibel et al. 2018), shocks (Randall et al. 2015; Li et al. 2017), cosmic rays (Loewenstein et al. 1991; Guo & Oh 2008; Fujita & Ohira 2011, 2012; Fujita et al. 2013; Pfrommer 2013; Jacob & Pfrommer 2017; Ruszkowski et al. 2017; Su et al. 2020), and mixing (Fujita et al. 2004; Hillel & Soker 2016, 2017, 2020; Fujita et al. 2020; Ueda et al. 2020, 2021), we represent it with a simple 'switch' for the sake of simplicity. This means that if the AGN feedback is strong enough, it switches off the development of thermal instability in the hot gas. If not, the instability sets in. Thus, we give the suppression factor as

$$f_{\text{sup}} = \exp(-L_{\text{AGN}}/L_{\text{cool}}) \quad (28)$$

in Equation (10). We assume that the hot gas is instantaneously heated by the AGN feedback. We have confirmed that the results are almost the same even if the heating is delayed by the sound crossing time of the hot gas over the galaxy ( $r_{\text{gal}}$ ).

### 2.6. Evolution equations for gas and stars

Evolution equations for the gas components are constructed based on the flow chart shown in Figure 1. For the interstellar cold gas, it is

$$\dot{M}_{g,i} = \dot{M}_{\text{cool}} - \frac{M_{g,i}}{t_{\text{dis,c}}(M_{g,i})}, \quad (29)$$

The first term on the right hand side is the supply from the hot gas, and the second term represents the disruption by star formation. The evolution of the circumnuclear disk gas is

$$\dot{M}_{g,d} = \dot{M}_{\text{sup}} - \dot{M}_{\text{BH}} - C_* M_{g,d}. \quad (30)$$

where

$$\dot{M}_{\text{sup}} = (1 - \epsilon_{*,c}(M_{g,i})) \frac{M_{g,i}}{t_{\text{dis,c}}(M_{g,i})}. \quad (31)$$

The first term on the right hand side of Equation (30) or  $\dot{M}_{\text{sup}}$  represents the supply from the cold interstellar gas. The second term is the gas flow toward the SMBH, and the third term is the consumption by star formation in the disk.

The mass of the stars formed in the interstellar cold gas  $M_{*,i}$  evolves as:

$$\dot{M}_{*,i} = (1 - R_{\text{ret}}) \frac{\epsilon_{*,c}(M_{g,i}) M_{g,i}}{t_{\text{dis,c}}(M_{g,i})}, \quad (32)$$

where  $R_{\text{ret}}$  is the fraction of the initial mass of a stellar population that is returned to the hot gas through mass loss from dying stars. In the instantaneous recycling approximation, it is  $R_{\text{ret}} \sim 0.5$  (Lacey et al. 2016). The right-hand side of Equation (32) corresponds to arrow (a) in Figure 1, although the fraction of  $R_{\text{ret}}$  goes to the hot gas (arrow (b)). The evolution of the mass of the stars formed in the circumnuclear disk  $M_{*,d}$  is

$$\dot{M}_{*,d} = (1 - R_{\text{ret}}) C_* M_{g,d}. \quad (33)$$

The right-hand side represents arrows (c) and (d).

Equations (32) and (33) show that both  $M_{*,i}$  and  $M_{*,d}$  are increasing functions of time. In our calculations,  $M_{*,d}$  far exceeds  $M_{g,d}$  over time (see Figure 5(a))<sup>1</sup>. However, it is unlikely that those stars remain in the disk, because a thin heavy stellar disk is unstable (Binney & Tremaine 2008). In reality, the stars are likely to be scattered through the gravitational interaction with the disk matter when the disk becomes gravitationally unstable even before the stellar mass dominates

in the disk. Thus, we assume that the stars represented by  $M_{*,d}$  are spherically and isothermally distributed at  $r < r_d$ . This means that the density profile of those stars is represented by  $\propto r^{-2}$  for  $r < r_d$ . Since the interstellar cold gas is distributed at  $r < r_i$  (Section 2.4.2), we also assume that the stars formed in the cold gas ( $M_{*,i}$ ) are isothermally distributed at  $r < r_i$ . The potential associated with both  $M_{*,i}$  and  $M_{*,d}$  is represented by  $\Phi_{\text{nstar}}(r)$  in Equation (3). However, we note that the contribution of  $\Phi_{\text{nstar}}(r)$  to the whole potential is minor in our calculations, and it hardly affects the results. For example, the temperature of the hot gas, which is given by Equation (7), changes only by  $\lesssim 0.1$  keV during our calculations.

### 3. MODEL BEHAVIOR

Although our model has many parameters (Table 1) and appears to be complicated, the state of the model galaxy virtually depends on a small handful of them. From Equations (10), (11), and (27), we obtain

$$\frac{L_{\text{AGN}}}{L_{\text{cool}}} = \frac{2 \mu m_p c^2 \epsilon_{\text{heat}}}{5 k T_{\text{hot}}} \frac{\dot{M}_{\text{BH}}}{\dot{M}_{\text{cool}}} f_{\text{sup}} \approx 2050 \frac{\dot{M}_{\text{BH}}}{\dot{M}_{\text{cool}}} f_{\text{sup}}. \quad (34)$$

In the last equation, we assume that  $\epsilon_{\text{heat}} = 0.02$  and  $k T_{\text{hot}} = 2.2$  keV. As is shown below,  $L_{\text{AGN}}$ ,  $\dot{M}_{\text{BH}}$ ,  $\dot{M}_{\text{cool}}$ , and  $f_{\text{sup}}$  often strongly fluctuate. Thus, we take their time averages, which are represented by  $\langle \rangle$ :

$$\frac{\langle L_{\text{AGN}} \rangle}{L_{\text{cool}}} \approx 2050 f_{\text{BH}} \langle f_{\text{sup}} \rangle, \quad (35)$$

where  $f_{\text{BH}} = \langle \dot{M}_{\text{BH}} \rangle / \langle \dot{M}_{\text{cool}} \rangle$ . We note that, while  $f_{\text{sup}} = \exp(-L_{\text{AGN}}/L_{\text{cool}})$  (Equation (28)),  $\langle f_{\text{sup}} \rangle$  is *not* generally equivalent to  $\exp(-\langle L_{\text{AGN}} \rangle / L_{\text{cool}})$ .

The gas flow and the AGN feedback of the model galaxy basically follow this relation. The main characteristic of the hot gas is  $L_{\text{cool}}$  (or equivalently  $\dot{M}_{\text{cool},0}$ ), which is fixed by giving the profile (Section 2.3). The fraction  $f_{\text{BH}}$  depends on the model of the interstellar cold gas (Section 2.4) and that of the circumnuclear disk (Section 2.5). The AGN luminosity  $\langle L_{\text{AGN}} \rangle$  also depends on the model of the circumnuclear disk.

### 4. RESULTS OF THE FIDUCIAL MODEL

In the fiducial model (FD model hereafter), we assume that the initial mass of the SMBH is  $M_{\text{BH}} = 3 \times 10^9 M_{\odot}$  and that of the cold interstellar gas is  $M_{g,i} = 1 \times 10^{10} M_{\odot}$ . These are typical values estimated or observed in clusters (e.g. McNamara et al. 2011; Olivares et al. 2019; Russell et al. 2019). At  $t = 0$ , there is no circumnuclear disk ( $M_{g,d} = M_{*,d} = 0$ ), and there are no stars

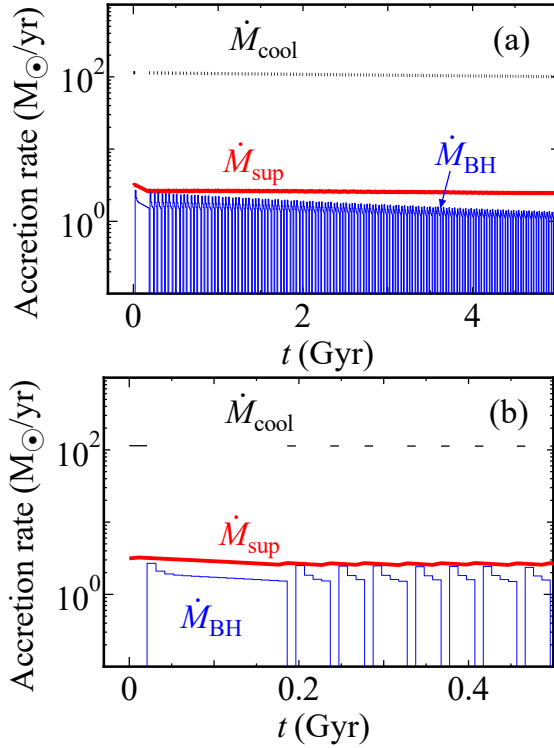
<sup>1</sup> This does not happen in previous studies (Kawakatu & Wada 2008; Wutschik et al. 2013), because their calculation times are shorter than ours.



**Table 2.** Model Results

Model	$\langle \dot{M}_{\text{BH}} \rangle$	$\dot{M}_{\text{cool},0}$	$\langle \dot{M}_{\text{cool}} \rangle$	$\langle L_{\text{AGN}} \rangle$	$L_{\text{cool}}$	$\langle f_{\text{sup}} \rangle$	$f_{\text{BH}}$
	$(M_{\odot} \text{ yr}^{-1})$	$(M_{\odot} \text{ yr}^{-1})$	$(M_{\odot} \text{ yr}^{-1})$	$(\text{erg s}^{-1})$	$(\text{erg s}^{-1})$		
FD	1.0	100	23	$1.2 \times 10^{45}$	$5.7 \times 10^{43}$	0.22	0.045
LM	1.0	100	23	$1.2 \times 10^{45}$	$5.7 \times 10^{43}$	0.22	0.045
ND	0.27	113	0.76	$3.1 \times 10^{44}$	$6.1 \times 10^{43}$	$6.7 \times 10^{-3}$	0.36
LE	1.7	1330	111	$1.9 \times 10^{45}$	$7.7 \times 10^{44}$	0.084	0.015
HE	0.14	0.88	0.72	$1.6 \times 10^{44}$	$4.8 \times 10^{41}$	0.82	0.19

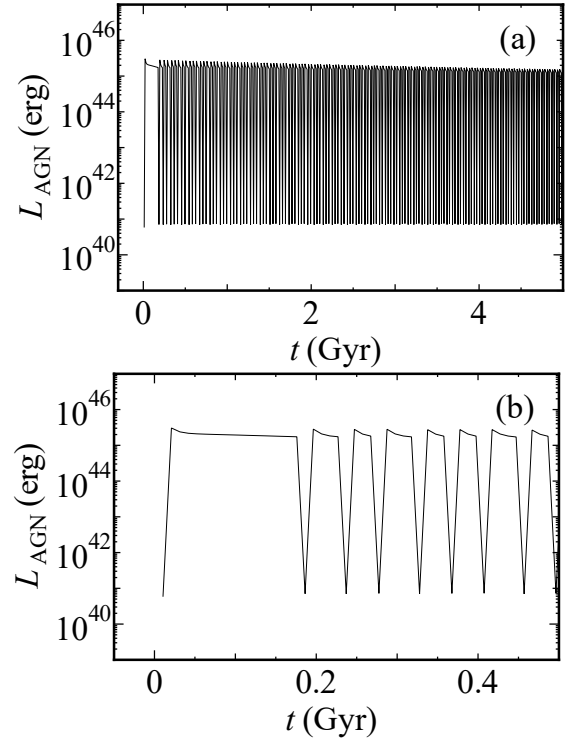
NOTE—Quantities are averaged over  $t = 3\text{--}5$  Gyr. Since  $\dot{M}_{\text{cool},0}$  and  $L_{\text{cool}}$  are almost time-independent, we do not add  $\langle \rangle$ .



**Figure 3.** Evolution of the cooling rate of the hot gas  $\dot{M}_{\text{cool}}$  (black dashed line), the supply rate toward the circumnuclear disk  $\dot{M}_{\text{sup}}$  (thick red solid line), and the accretion rate toward the SMBH  $\dot{M}_{\text{BH}}$  (thin blue solid line) for the FD model for  $t < 5$  Gyr (a) and for  $t < 0.5$  Gyr (b). Note that the length of each black dash ( $\dot{M}_{\text{cool}}$ ) reflects an inactive period of the AGN. The data of  $\dot{M}_{\text{cool}} \sim 0$  are not shown for clarity. The mass-supply rate  $\dot{M}_{\text{sup}}$  does not show rapid violent changes.

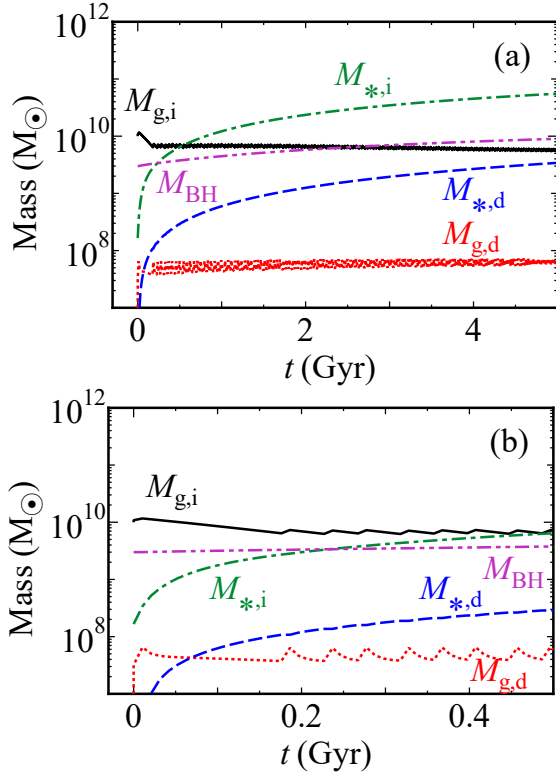
in the cold interstellar gas ( $M_{*,i} = 0$ ). We calculate the evolution of the system by  $t = 5$  Gyr. We set the time step of the calculations for  $\Delta t = 2\pi/\Omega(r_d) \sim 10^7$  yr, because our disk model is a one-zone model, and it cannot treat shorter time-scale phenomena that may happen inside the disk.

Figure 3 shows the mass transfer among gas components (see Figure 1). The mass accretion rate toward



**Figure 4.** Variation of AGN power for the FD model for  $t < 5$  Gyr (a) and for  $t < 0.5$  Gyr (b).

the SMBH ( $\dot{M}_{\text{BH}}$ ) and the cooling rate of the hot gas ( $\dot{M}_{\text{cool}}$ ) show rapid violent changes at  $t \gtrsim 0.2$  Gyr. The variation of  $\dot{M}_{\text{BH}}$  reflects the switching between the on and off states of the gravitational instability of the circumnuclear disk as follows. If the disk becomes unstable ( $\Sigma_d > \Sigma_{\text{crit}}$ ), star formation in the disk is activated. As a result, strong turbulence develops in the disk, which leads to the efficient transport of angular momentum and causes an increase in  $\dot{M}_{\text{BH}}$  (Section 2.5.4). The larger  $\dot{M}_{\text{BH}}$  causes a decrease in the mass of the disk gas  $M_{\text{g},d}$ , which stabilizes the disk ( $\Sigma_d < \Sigma_{\text{crit}}$ ). During this stable state, the turbulence in the disk is not strong, and  $\dot{M}_{\text{BH}}$  decreases. On the other hand, the disk mass increases because of the stable supply from the inter-



**Figure 5.** Evolution of the masses of the interstellar cold gas  $M_{g,i}$  (black solid line), the circumnuclear disk gas  $M_{g,d}$  (red dotted line), the stars formed in the interstellar cold gas  $M_{*,i}$  (blue dashed line), the stars formed in the circumnuclear disk  $M_{*,d}$  (green dashed-dotted line), and the SMBH  $M_{BH}$  (violet dashed-two dotted line) for model FD for  $t < 5$  Gyr (a) and for  $t < 0.5$  Gyr (b).

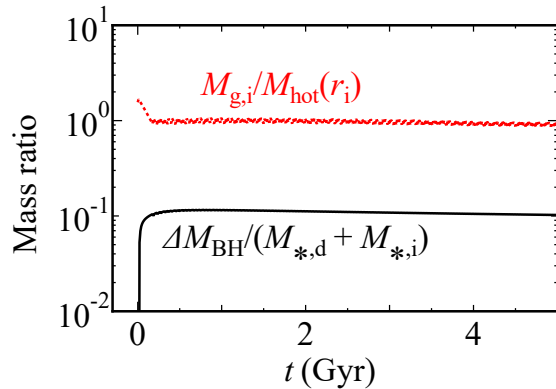


**Figure 6.** Black solid line shows the ratio of the increment of the black hole mass  $\Delta M_{BH} \equiv M_{BH}(t) - M_{BH}(0)$  to the mass of newly formed stars  $M_{*,i} + M_{*,g}$  for model FD. Red dotted line shows the ratio of the mass of the cold interstellar gas  $M_{g,i}$  to that of the hot gas within  $r_i$ , which is represented by  $M_{hot}(r_i)$ .

stellar cold gas ( $\dot{M}_{sup}$  in Figure 3), and then the disk becomes unstable again. This cycle continues to repeat. Since the disk adjusts the AGN fueling so that the condition of  $\Sigma_d \sim \Sigma_{crit}$  is kept, we may call the disk an 'adjusting valve' of AGN feedback.

While a larger  $\dot{M}_{BH}$  boosts  $L_{AGN}$  (Equation (27)), it suppresses  $\dot{M}_{cool}$  (Equations (10) and (28)). Thus, while  $L_{AGN}$  and  $\dot{M}_{BH}$  are correlated (Figures 3 and 4),  $\dot{M}_{cool}$  and  $\dot{M}_{BH}$  are inversely correlated (Figure 3). In our model,  $L_{AGN}$  just works as a 'switch' of the cooling of the hot gas (Equation (28)). Thus, the value of  $\epsilon_{heat}$  in Equation (27) is not important as long as  $L_{AGN} \gg L_{cool} \sim 6 \times 10^{43} \text{ erg s}^{-1}$  (Table 2) or  $L_{AGN} \ll L_{cool}$ . Even if  $\epsilon_{heat} = 0.002$  instead of 0.02 in the FD model, the results are almost the same except that the AGN luminosity during the active phase decreases down to  $L_{AGN} \sim 10^{44} \text{ erg s}^{-1}$ .

The gas supply rate  $\dot{M}_{sup}$  does not show rapid sharp changes because it depends on  $M_{g,i}$  but not on  $\dot{M}_{cool}$  (Equation (31)). This means that the impact of abrupt changes of the hot-gas cooling rate is alleviated by the interstellar cold gas, and it does not directly affect the circumnuclear disk. Thus, the interstellar cold gas works as a 'buffer' that contributes the stability of AGN feedback.

Figure 5 shows that the mass of the interstellar cold gas  $M_{g,i}$  decreases at  $t \lesssim 0.2$  Gyr, and then it becomes almost constant at  $t \gtrsim 0.2$  Gyr. During the initial stage ( $t \lesssim 0.2$  Gyr), the circumnuclear disk is almost always unstable because the slightly higher gas-supply rate ( $\dot{M}_{sup}$  in Figure 3) leads to a larger  $\Sigma_d$ . Thus, the AGN stays in an active phase ( $L_{AGN} \sim 10^{45} \text{ erg s}^{-1}$  in Figure 4), and the cooling of the hot gas  $\dot{M}_{cool}$  is strongly suppressed (Equation (28)). As the mass of the cold interstellar gas  $M_{g,i}$  decreases,  $\dot{M}_{sup}$  and  $\Sigma_d$  also slightly decline. In time, the circumnuclear disk becomes intermittently stable, and the oscillation of  $L_{AGN}$  begins ( $t \gtrsim 0.2$  Gyr in Figure 4). The final values of  $M_{g,i} \sim 10^{10} M_{\odot}$  and  $M_{g,d} \sim 10^8 M_{\odot}$  are consistent with those for NGC 1275 at the center of the Perseus cluster (Salomé et al. 2006; Lim et al. 2008; Nagai et al. 2019), although this may be a result of our choice of parameters related to the disk stability. We note that the mass of the interstellar cold gas  $M_{g,i}$  is sensitive to the cloud disruption time  $t_{dis,c}$  and the star formation efficiency  $\epsilon_{*,c}$ . In the FD model, the disruption time is  $t_{dis,c} \gtrsim 10^8 \text{ yr}$ , which is much longer than that for the giant molecular clouds in the Milky Way ( $t_{dis,c} \sim 10^7 \text{ yr}$ ; Elmegreen & Efremov 1997). This reflects that  $t_{dis,c}$  is an increasing function of the mass  $M_{g,i}$ , and  $M_{g,i}$  of the model galaxy is much larger than the mass of the giant molecular clouds in the Milky Way ( $\sim 10^5 M_{\odot}$ ; see Figure 2).

Our model shows that the huge masses ( $\gtrsim 10^9 M_\odot$ ) of observed molecular gas in massive elliptical galaxies is a consequence of the very long disruption time of the gas, although the larger  $\epsilon_{*,c}$  partially cancels the effect.

Using the time-averaged ( $t = 3\text{--}5$  Gyr) values presented in Table 2, one can show that Equation (35) is valid within  $\sim 1\%$  accuracy. This suggests that the final state of the galaxy is actually determined by a small number of factors, such as the cooling rate of the hot gas ( $L_{\text{cool}}$ )<sup>2</sup>, the disruption time and the star formation efficiency of the interstellar cold gas ( $t_{\text{dis},c}$  and  $\epsilon_{*,c}$ ), and the stability condition of the circumnuclear disk that is controlled by the star formation in the disk.

The duty cycle of the AGN activity depends on the time step  $\Delta t$ . However, we have confirmed that the overall evolution of the system and the quantities such as the masses of gas and stellar components are not sensitive to the time step as long as  $\Delta t \lesssim 10^7$  yr. This is because the evolution is mainly determined by the ratio of the total time when the disk is unstable to that when the disk is stable. This ratio is not sensitive to  $\Delta t$ , and it is around 4 for the FD model. We note that, in Figure 3(a), the cooling rate appears to be  $\dot{M}_{\text{cool}} \sim 100 M_\odot \text{ yr}^{-1} \sim \dot{M}_{\text{cool},0}$  (Table 2). However, it actually rapidly changes, which is clearly expressed in a magnified figure (Figure 3(b)). Since AGN feedback suppresses the cooling rate down to  $\dot{M}_{\text{cool}} \sim 0$  for  $\sim 80\%$  of the total calculation time, the time-averaged cooling rate is  $\langle \dot{M}_{\text{cool}} \rangle \sim 20 M_\odot \text{ yr}^{-1}$  (Table 2). While the evolution of the cold interstellar gas is determined by  $\langle \dot{M}_{\text{cool}} \rangle$ , it is insensitive to the period of the rapid change of  $\dot{M}_{\text{cool}}$ . This may mean that the results do not largely depend on the details of the AGN feedback as long as the feedback significantly suppresses the cooling rate  $\dot{M}_{\text{cool}}$ .

Since the stars formed in the galaxy accumulate, the stellar masses  $M_{*,i}$  and  $M_{*,d}$  increase as time goes by and exceed the gas masses  $M_{g,i}$  and  $M_{g,d}$ , respectively (Figure 5). However, the mass of the newly formed stars,  $M_{*,i} + M_{*,g}$ , is much smaller than that of the old stars that had already existed at  $t = 0$ . In fact, because the old stars are the origin of the potential  $\Phi_{\text{ISO}}$  (Equation (1)), their total mass can be calculated from  $\Phi_{\text{ISO}}(r_{\text{gal}})$ , and it is  $\sim 3 \times 10^{12} M_\odot$ . In Figure 6,

we present the ratio of the increment of the black hole mass  $\Delta M_{\text{BH}} \equiv M_{\text{BH}}(t) - M_{\text{BH}}(0)$  to  $M_{*,i} + M_{*,g}$ . For  $t \gtrsim 0.2$  Gyr, the ratio is almost constant ( $\sim 0.1$ ). Figure 6 also shows the ratio of the mass of the cold interstellar mass  $M_{g,i}$  to that of the hot gas where the cold gas coexists  $M_{\text{hot}}(r_i)$ . For  $t \gtrsim 0.2$  Gyr, the ratio is almost constant and the value is close to one, which is consistent with the results of recent ALMA observations (Russell et al. 2019).

## 5. DISCUSSION

### 5.1. Roles of the interstellar gas and the circumnuclear disk

In order to investigate the role of the cold interstellar gas, we study the case where the environment of the galaxy suddenly changes. In Figure 7, we show the results when we intentionally set the cooling rate of the hot gas at  $\dot{M}_{\text{cool}} = 0$  for  $t > 3$  Gyr; the other parameters are the same as those in the FD model. Figure 7(b) shows that the AGN continues to be active for  $\sim 0.7$  Gyr even after the cooling of the hot gas stops. This is because the mass supply from the cold interstellar gas to the nuclear disk continues as long as  $M_{g,i} > 0$  (Figure 7(c)). The decline time of  $M_{g,i}$  is basically determined by  $t_{\text{dis},c}$ . This means that the cold interstellar gas works as a 'fuel tank' for the AGN, which could be likened to a magma chamber for a volcano. This mechanism may be important in terms of the stability of AGN feedback. For example, if the host cluster of the central galaxy undergoes a cluster merger, the hot gas may suddenly be heated, and its cooling may be halted. Even if this happens, the fueling of the AGN is not immediately interrupted by this environmental catastrophe. Thus, the interstellar cold gas may also work as a 'buffer'.

The evolution of the system does not depend on the initial condition of the interstellar cold gas. Figure 8 shows the results when  $M_{g,i}(t=0) = 1 \times 10^9 M_\odot$  instead of  $1 \times 10^{10} M_\odot$  in the FD model. We refer to this low-initial-mass model as model LM. The mass  $M_{g,i}$  rapidly increases for  $t < 0.2$  Gyr, and then the evolution of the galaxy is almost the same as that of the FD model (Figures 3–5). In fact, Table 2 shows that parameters related to the mass flows and powers are the exactly same as those for the FD model. This indicates that the state of the galaxy is simply described by Equation (35).

Figure 9 shows the results when there is no circumnuclear disk (model ND). We consider this situation from a physical point of view. In this model, the interstellar cold gas directly fuels the SMBH and we set

$$\dot{M}_{\text{BH}} = \dot{M}_{\text{sup}} = (1 - \epsilon_{*,c}(M_{g,i})) \frac{M_{g,i}}{t_{\text{dis},c}(M_{g,i})}, \quad (36)$$

<sup>2</sup> To be exact,  $L_{\text{cool}}$  (and  $M_{\text{cool},0}$ ) slightly decreases ( $\sim 10\%$ ) during the calculation as the temperature  $T_{\text{hot}}$  slightly increases because stars formed in the interstellar cold gas and the circumnuclear disk deepen the gravitational potential (Equation (3)). The increase in  $T_{\text{hot}}$  leads to a decrease in  $r_{\text{cool}}$ , which is determined by  $t_{\text{cool}} \propto T_{\text{hot}}/(\rho(r_{\text{cool}})\Lambda(T_{\text{hot}}, Z))$  (Section 2.4.2). In Table 2,  $M_{\text{cool},0}$  and  $L_{\text{cool}}$  are also the averaged values although we do not explicitly show  $\langle \rangle$ .

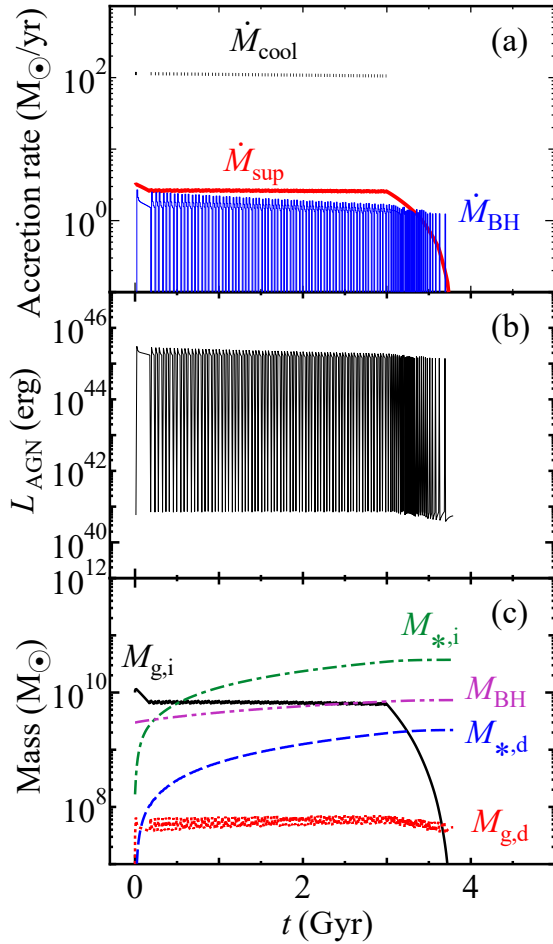


**Figure 7.** Results when the cooling of the hot gas suddenly stops at  $t > 3$  Gyr in model FD. (a) Same as Figure 3(a). (b) Same as Figure 4(a). (c) Same as Figure 5(a).

from Equation (31) instead of Equation (24). In contrast with the FD model (Figures 3(a) and 4(a)), the average gas supply rate ( $\langle \dot{M}_{\text{BH}} \rangle = \langle \dot{M}_{\text{sup}} \rangle$ ) is low (Table 2), and the AGN power  $L_{\text{AGN}}$  does not show rapid variation because there is no disk instability. Moreover, the mass of the interstellar cold gas ( $M_{\text{g},i} < 10^8 M_{\odot}$ ; Figure 9(c)) is much smaller than that in the FD model ( $M_{\text{g},i} > 10^9 M_{\odot}$ ; Figure 5). This is because the AGN activity *constantly* suppresses the cooling of the hot gas, and the average suppression factor  $\langle f_{\text{sup}} \rangle$  is much smaller than that for the FD model (Table 2). This indicates that the presence or absence of the small circumnuclear disk ( $r_{\text{disk}} \sim 0.4$  kpc) can affect the whole galaxy ( $r_{\text{gal}} \sim 30$  kpc) through AGN feedback and can change the amount of the cold gas in the galaxy. Equation (35) is established with a few percent accuracy for the values in Table 2.

In reality, even if the circumnuclear disk is destroyed by a galaxy collision (Miki et al. 2021), it will soon be rebuilt if there is interstellar cold gas. For example, the

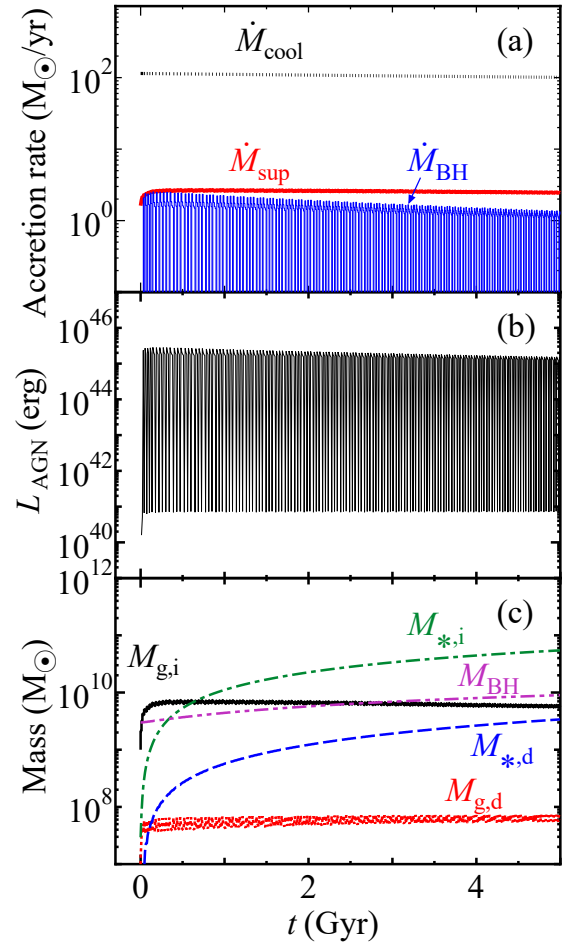


**Figure 8.** Results when the initial mass of the interstellar cold gas is  $M_{\text{g},i} = 1 \times 10^9 M_{\odot}$  (model LM). (a) Same as Figure 3(a). (b) Same as Figure 4(a). (c) Same as Figure 5(a).

disk mass  $M_{\text{g},d}$  grows rapidly from  $M_{\text{g},d} = 0$  at  $t \sim 0$ , as is shown in Figure 5(b). However, if the cold gas has no angular momentum and the disk is not formed, the situation similar to Figure 9 may be realized.

## 5.2. Entropy of the hot gas and the interstellar cold gas

Observations have indicated that cold gas (molecular gas) and warm gas ( $\text{H}\alpha$ -emitting gas) tend to be discovered in galaxies with low-entropy hot gas (Cavagnolo et al. 2008; Rafferty et al. 2008; Sanderson et al. 2009; Main et al. 2017). This implies a strong connection between the entropy and the formation of the interstellar cold gas. Motivated by these observations, we study the connection using our semianalytical model.

Here, we define the specific entropy as  $K \equiv kTn_e^{-2/3}$  and refer to the value at  $r = r_{\text{gal}} = 30$  kpc as  $K_{30}$ . Hogan et al. (2017b) showed that  $K_{30} \sim 25$ – $60$  keV  $\text{cm}^2$  for clusters with  $\text{H}\alpha$  nebular emission and  $K_{30} \gtrsim 60$  keV  $\text{cm}^2$  for those without  $\text{H}\alpha$  nebular emission. We note that the entropies at the centers of the for-

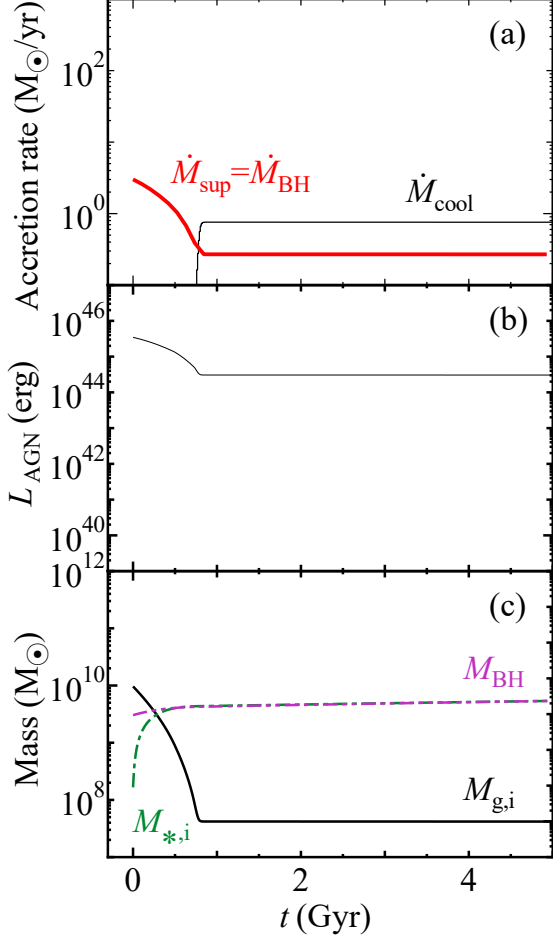


**Figure 9.** Results when there is no circumnuclear disk (model ND). (a) Same as Figure 3(a) except that  $\dot{M}_{\text{cool}}$  is represented by the thin black solid line. (b) Same as Figure 4(a). (c) Same as Figure 5(a). Since there is no disk,  $M_{\text{g,d}}$  and  $M_{*,\text{d}}$  are not shown.

mer are  $K \lesssim 30 \text{ keV cm}^2$  (Hogan et al. 2017b). Thus, the condition of  $K_{30} \sim 25\text{--}60 \text{ keV cm}^2$  is roughly equivalent to the known condition of gas cooling ( $K \lesssim 30 \text{ keV cm}^2$  at  $r \sim 0$ ; Cavagnolo et al. 2008; Rafferty et al. 2008; Sanderson et al. 2009).

In the FD model,  $K_{30} \sim 30 \text{ keV cm}^2$  and the value of  $n_e$  at  $r = r_{\text{gal}} = 30 \text{ kpc}$ , namely  $n_{e,0}$ , is  $0.02 \text{ cm}^{-3}$  (Equation (4)). In this subsection, we change the value of  $n_{e,0}$ , while other parameters are the same as those for the FD model. Figure 10 shows the evolution when  $n_{e,0} = 0.03 \text{ cm}^{-3}$ , which means  $K_{30} \sim 24 \text{ keV cm}^2$ . We refer to this low-entropy model as model LE. In this case, the intrinsic radiative cooling rate of the hot gas ( $L_{\text{cool}}$  or equivalently  $M_{0,\text{cool}}$ ) is much larger than that for the FD model (Table 2). Although the constantly large AGN power  $\langle L_{\text{AGN}} \rangle$  suppresses the actual gas cooling, the average gas cooling rate  $\langle \dot{M}_{\text{cool}} \rangle$  is still larger than that for the FD model (Table 2). Thus,

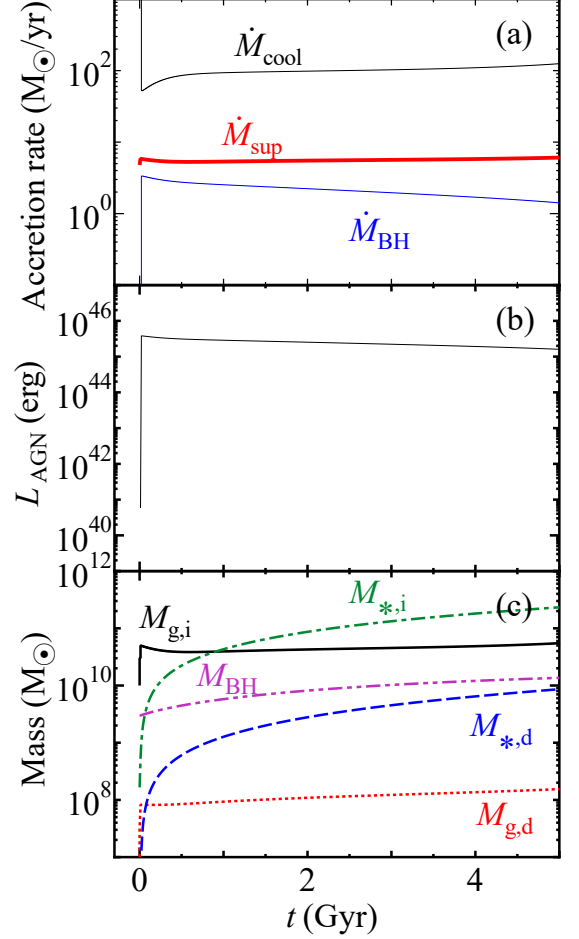


**Figure 10.** Results for  $n_{e,0} = 0.03 \text{ cm}^{-3}$ , which means  $K_{30} \sim 22 \text{ keV cm}^2$  (model LE). (a) Same as Figure 3(a) except that  $\dot{M}_{\text{cool}}$  is represented by the thin black solid line. (b) Same as Figure 4(a). (c) Same as Figure 5(a).

the mass of the interstellar cold gas keeps a large value ( $M_{\text{g,i}} \sim 5 \times 10^{10} M_{\odot}$ ; Figure 10) in comparison with that for the FD model ( $M_{\text{g,i}} \sim 6 \times 10^9 M_{\odot}$  for  $t \gtrsim 1 \text{ Gyr}$ ; Figure 5). As a result, the mass flow rate toward the circumnuclear disk is high, which means that the disk is constantly heavy and unstable. Thus, the disk no longer works as the adjusting valve of mass accretion toward the SMBH. The resultant large  $\dot{M}_{\text{BH}}$  supports the large  $L_{\text{AGN}}$ . We have confirmed that Equation (35) is approximately ( $\sim 5\%$ ) valid for the values in Table 2. In our model, the cold gas that is not swallowed by the SMBH is consumed in star formation. The star formation rate of the galaxy is given by

$$\dot{M}_{*} = \frac{\epsilon_{*,\text{c}}(M_{\text{g,i}})M_{\text{g,i}}}{t_{\text{dis,c}}(M_{\text{g,i}})} + C_{*}M_{\text{g,d}}, \quad (37)$$

and it is relatively high ( $\dot{M}_{*} \sim 100 M_{\odot} \text{ yr}^{-1}$ ) compared with the average value for the FD model ( $\dot{M}_{*} \sim 20 M_{\odot} \text{ yr}^{-1}$  for  $t \gtrsim 1 \text{ Gyr}$ ). The results are at least qual-



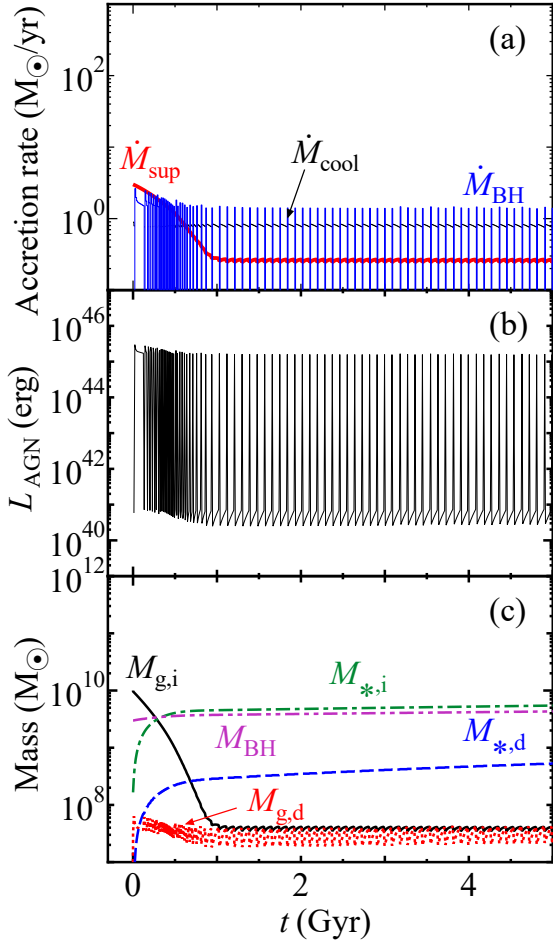


**Figure 11.** Results for  $n_{e,0} = 0.01 \text{ cm}^{-3}$ , which means  $K_{30} \sim 46 \text{ keV cm}^2$  (model HE). (a) Same as Figure 3(a) except that  $\dot{M}_{\text{cool}}$  is represented by the thin black solid line. (b) Same as Figure 4(a). (c) Same as Figure 5(a).

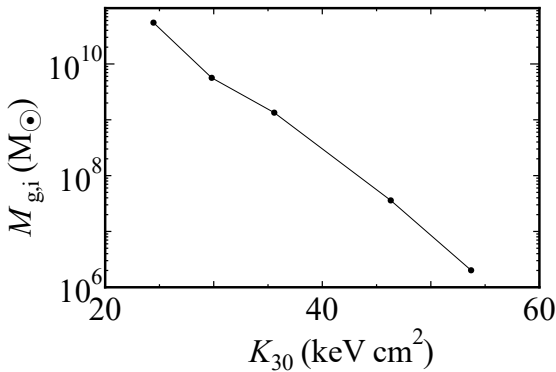


**Figure 12.** Relation between the specific entropy at  $r = 30 \text{ kpc}$  ( $K_{30}$ ) and the mass of the interstellar cold gas ( $M_{g,i}$ ) at  $t = 5 \text{ Gyr}$ .

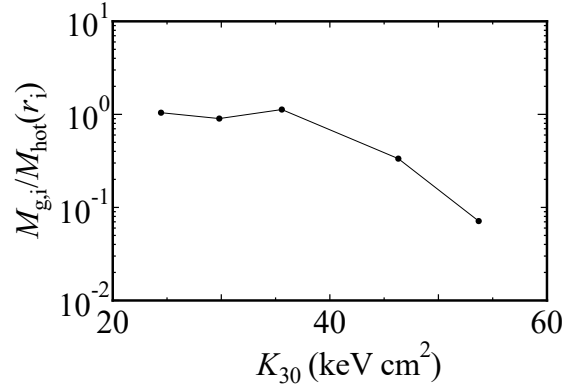


**Figure 13.** Relation between the specific entropy at  $r = 30 \text{ kpc}$  ( $K_{30}$ ) and the ratio of the mass of the cold interstellar gas ( $M_{g,i}$ ) to that of the hot gas ( $M_{\text{hot}}(r_i)$ ) at  $t = 5 \text{ Gyr}$ .

itatively similar to what is happening in the Phoenix cluster. This cluster has an exceptionally low entropy ( $K_{30} \lesssim 20 \text{ keV cm}^2$ ; McDonald et al. 2019; Kitayama et al. 2020), a high star formation rate ( $\dot{M}_* \sim 500\text{--}600 M_\odot \text{ yr}^{-1}$ ; McDonald et al. 2015; Mittal et al. 2017), and an active AGN ( $L_{\text{AGN}} \sim 10^{46} \text{ erg s}^{-1}$ ; McDonald et al. 2019; Akahori et al. 2020). Since Figure 10 shows that the system is stable, the Phoenix cluster may keep its unusual state unless its environment (e.g. the hot gas) changes.

In Figure 11, we present the results when  $n_{e,0} = 0.01 \text{ cm}^{-3}$ , which means  $K_{30} \sim 46 \text{ keV cm}^2$ . We refer to this high-entropy model as model HE. The low density and the high entropy mean that the cooling rate of the hot gas is intrinsically low ( $L_{\text{cool}}$  or  $\dot{M}_{\text{cool},0}$  in Table 2). The actual cooling rate of the hot gas  $\dot{M}_{\text{cool}}$  (Figure 11(a)) is also low compared with that of the FD model (Figure 3(a) and Table 2). As a result, the mass of the interstellar cold gas  $M_{g,i}$  decreases at  $t \lesssim 1 \text{ Gyr}$ ; the decline time of  $M_{g,i}$  is mainly determined by  $t_{\text{dis,c}}$ . Then  $M_{g,i}$  maintains a small value ( $M_{g,i} \sim 4 \times 10^7 M_\odot$ ; Figure 11(c)). Since the gas supply to the circumnuclear disk ( $\dot{M}_{\text{sup}}$ ) is also reduced at  $t \gtrsim 1 \text{ Gyr}$  (Figure 11(a)), the disk gas mass  $M_{g,d}$  (Figure 11(c)) and the surface density  $\Sigma_d$  are kept low. Thus, the disk is stable most of the time, and the activity of the AGN is generally low ( $L_{\text{AGN}} \sim 2\text{--}6 \times 10^{40} \text{ erg s}^{-1}$ ; Figure 11(b)), although the AGN often shows short bursts ( $L_{\text{AGN}} \sim 10^{45} \text{ erg s}^{-1}$ ) because of instantaneous disk instabilities. The star formation rate at  $t \gtrsim 1 \text{ Gyr}$  is also very small ( $\dot{M}_* \lesssim 1 M_\odot \text{ yr}^{-1}$ ). Again, we have confirmed that the final state of the system is represented by Equation (35) with a few percent accuracy using the values in Table 2.

We also study the evolution when the entropy is even higher ( $n_{e,0} = 0.006 \text{ cm}^{-3}$  and  $K_{30} \sim 65 \text{ keV cm}^2$ ). In

this case, the interstellar cold gas disappears ( $M_{g,i} \rightarrow 0$ ) by  $t \sim 1$  Gyr, and the AGN activity completely cease. The Virgo cluster (M87) may be close to this situation (Simionescu et al. 2018) because of the high entropy of  $K_{30} \sim 70 \text{ keV cm}^2$  (Matsushita et al. 2002).

In Figure 12, we summarize the relation between  $K_{30}$  and the mass of the interstellar cold gas  $M_{g,i}$  at  $t = 5$  Gyr. Figure 13 shows the relation between  $K_{30}$  and the ratio of the mass of the cold interstellar gas,  $M_{g,i}$ , to that of the hot gas,  $M_{\text{hot}}(r_i)$ , at  $t = 5$  Gyr. The evolution of the ratio was shown in Figure 6 in the case of the FD model ( $K_{30} \sim 30 \text{ keV cm}^2$ ). In Figure 13, while the ratio is  $\sim 1$  for  $K_{30} \lesssim 40 \text{ keV cm}^2$ , it decreases for  $K_{30} \gtrsim 40 \text{ keV cm}^2$ . This trend could be discussed in future observations.

The results in this subsection clearly indicate that the evolution of the interstellar cold gas and AGN feedback induced by the cold gas are very sensitive to the entropy of the hot gas. Equation (35) suggests that  $L_{\text{cool}}$  is a fundamental factor that determines the state of the system, and that the entropy is one manifestation of that because the entropy is anticorrelated with  $L_{\text{cool}}$ . The entropy we studied ( $K_{30} \sim 30 \text{ keV cm}^2$ ) corresponds to our threshold cooling time  $t_{\text{cool}} = 0.7$  Gyr (Section 2.4.2), which is comparable to the actual survival time of the interstellar cold gas ( $\sim 0.7$  Gyr; Section 5.1 and Figure 7). This may mean that the threshold cooling time reflects the condition that the cooling of the hot gas compensates the dissipation of the interstellar cold gas. Since the profile of the hot gas is based on the boundary conditions at  $r_{\text{gal}} = 30$  kpc (Section 2.3), our results may indicate that the surrounding intracluster gas of the host cluster regulates the formation of the interstellar cold gas and AGN feedback. Since cluster mergers can significantly change the distribution of the intracluster gas, they can affect the mass of the interstellar cold gas. Moreover, if an enormously powerful AGN explosion boosts the entropy beyond the boundary ( $r > r_{\text{gal}}$ ), it may have a similar effect on the interstellar cold gas.

## 6. CONCLUSION

We have studied the role of massive molecular gas clouds in AGN feedback in giant elliptical galaxies at the centers of galaxy clusters using a semianalytical model. We constructed the model based on representative models for the evolution of the massive molecular gas (interstellar cold gas) and the circumnuclear disk. We consider the destruction of the interstellar cold gas by star formation, and we also take into account the gravitational instabilities of the circumnuclear disk. Our model reproduced the basic properties of the interstellar cold gas and the circumnuclear disk, such as their masses. We

found that the final state of a galaxy is represented by a simple relation (Equation (35)), which reflects three key factors: (1) the stability condition of the circumnuclear disk, (2) the disruption time and the star formation efficiency of the interstellar cold gas, and (3) the cooling rate or the X-ray luminosity of the hot gas ( $L_{\text{cool}}$ ). The role of each factor can be summarized as follows.

1. The circumnuclear disk tends to stay at the boundary between stable and unstable states. This works as an 'adjusting valve' and regulates mass accretion toward the SMBH and AGN feedback.
2. The long disruption time of the interstellar cold gas is the reason for its large mass. The interstellar cold gas serves as a 'fuel tank' in AGN feedback. Even if the cooling of the galactic hot gas is halted for some reason (e.g. cluster mergers), the interstellar cold gas can supply its gas to the circumnuclear disk and maintain AGN activity for  $\gtrsim 0.5$  Gyr.
3. The luminosity  $L_{\text{cool}}$  regulates the mass supply to the interstellar cold gas; larger  $L_{\text{cool}}$  means a larger supply rate. Since the entropy and the cooling time of the hot gas tend to be smaller for clusters with larger  $L_{\text{cool}}$ , the mass of the interstellar cold gas increases as the entropy or equivalently the cooling time of the hot gas decreases. We confirmed that the small entropy of the hot gas at the cluster centers ( $\lesssim 30 \text{ keV cm}^2$  at  $r \sim 0$ ) or the short cooling time ( $\lesssim 1$  Gyr) is a key condition for the existence of the massive molecular gas clouds in the central galaxy, as previous studies suggested. We found that if the entropy is much smaller than  $30 \text{ keV cm}^2$ , the star formation and the AGN become very active, which has actually been observed in the Phoenix cluster. The ratio of the mass of the interstellar cold gas to that of the hot gas is close to one when the entropy of the hot gas is relatively small. The critical cooling time of the hot gas ( $\lesssim 1$  Gyr) may be related to the long disruption time of the interstellar cold gas.

Since our model is very simple, particularly for the hot gas and AGN feedback, more sophisticated models and/or numerical simulations would be desirable. For example, semianalytical models that include the evolution of hot gas profiles and numerical simulations that resolve circumnuclear disks would be useful.

We would like to thank the anonymous referee for a constructive report. This work was supported by JSPS KAKENHI No.18K03647, 20H00181 (Y.F.), 19K03918 (N.K.), and JP18K03709 (H.N.)

## REFERENCES

- Akahori, T., Kitayama, T., Ueda, S., et al. 2020, PASJ, 72, 62, doi: [10.1093/pasj/psaa039](https://doi.org/10.1093/pasj/psaa039)
- Balbus, S. A., & Hawley, J. F. 1991, ApJ, 376, 214, doi: [10.1086/170270](https://doi.org/10.1086/170270)
- Barai, P., Proga, D., & Nagamine, K. 2012, MNRAS, 424, 728, doi: [10.1111/j.1365-2966.2012.21260.x](https://doi.org/10.1111/j.1365-2966.2012.21260.x)
- Binney, J., & Tremaine, S. 2008, Galactic Dynamics: Second Edition
- Bourne, M. A., & Sijacki, D. 2017, MNRAS, 472, 4707, doi: [10.1093/mnras/stx2269](https://doi.org/10.1093/mnras/stx2269)
- Bourne, M. A., Sijacki, D., & Puchwein, E. 2019, MNRAS, 490, 343, doi: [10.1093/mnras/stz2604](https://doi.org/10.1093/mnras/stz2604)
- Cavagnolo, K. W., Donahue, M., Voit, G. M., & Sun, M. 2008, ApJL, 683, L107, doi: [10.1086/591665](https://doi.org/10.1086/591665)
- Churazov, E., Forman, W., Jones, C., & Böhringer, H. 2000, A&A, 356, 788. <https://arxiv.org/abs/astro-ph/0002375>
- Ciotti, L., & Ostriker, J. P. 2007, ApJ, 665, 1038, doi: [10.1086/519833](https://doi.org/10.1086/519833)
- Ciotti, L., Ostriker, J. P., & Proga, D. 2010, ApJ, 717, 708, doi: [10.1088/0004-637X/717/2/708](https://doi.org/10.1088/0004-637X/717/2/708)
- Ciotti, L., Pellegrini, S., Negri, A., & Ostriker, J. P. 2017, ApJ, 835, 15, doi: [10.3847/1538-4357/835/1/15](https://doi.org/10.3847/1538-4357/835/1/15)
- Crawford, C. S., Allen, S. W., Ebeling, H., Edge, A. C., & Fabian, A. C. 1999, MNRAS, 306, 857, doi: [10.1046/j.1365-8711.1999.02583.x](https://doi.org/10.1046/j.1365-8711.1999.02583.x)
- David, L. P., Lim, J., Forman, W., et al. 2014, ApJ, 792, 94, doi: [10.1088/0004-637X/792/2/94](https://doi.org/10.1088/0004-637X/792/2/94)
- Davies, R. I., Müller Sánchez, F., Genzel, R., et al. 2007, ApJ, 671, 1388, doi: [10.1086/523032](https://doi.org/10.1086/523032)
- Edge, A. C. 2001, MNRAS, 328, 762, doi: [10.1046/j.1365-8711.2001.04802.x](https://doi.org/10.1046/j.1365-8711.2001.04802.x)
- Elmegreen, B. G. 1989, ApJ, 338, 178, doi: [10.1086/167192](https://doi.org/10.1086/167192)
- Elmegreen, B. G., & Efremov, Y. N. 1997, ApJ, 480, 235, doi: [10.1086/303966](https://doi.org/10.1086/303966)
- Fabian, A. C. 1994, ARA&A, 32, 277, doi: [10.1146/annurev.aa.32.090194.001425](https://doi.org/10.1146/annurev.aa.32.090194.001425)
- . 2012, ARA&A, 50, 455, doi: [10.1146/annurev-astro-081811-125521](https://doi.org/10.1146/annurev-astro-081811-125521)
- Fabian, A. C., Sanders, J. S., Taylor, G. B., et al. 2006, MNRAS, 366, 417, doi: [10.1111/j.1365-2966.2005.09896.x](https://doi.org/10.1111/j.1365-2966.2005.09896.x)
- Fabian, A. C., Walker, S. A., Russell, H. R., et al. 2017, MNRAS, 464, L1, doi: [10.1093/mnrasl/slz170](https://doi.org/10.1093/mnrasl/slz170)
- Fujita, Y., Cen, R., & Zhuravleva, I. 2020, MNRAS, 494, 5507, doi: [10.1093/mnras/staa1087](https://doi.org/10.1093/mnras/staa1087)
- Fujita, Y., Kimura, S., & Ohira, Y. 2013, MNRAS, 432, 1434, doi: [10.1093/mnras/stt563](https://doi.org/10.1093/mnras/stt563)
- Fujita, Y., Matsumoto, T., & Wada, K. 2004, ApJL, 612, L9, doi: [10.1086/424483](https://doi.org/10.1086/424483)
- Fujita, Y., & Ohira, Y. 2011, ApJ, 738, 182, doi: [10.1088/0004-637X/738/2/182](https://doi.org/10.1088/0004-637X/738/2/182)
- . 2012, ApJ, 746, 53, doi: [10.1088/0004-637X/746/1/53](https://doi.org/10.1088/0004-637X/746/1/53)
- . 2013, MNRAS, 428, 599, doi: [10.1093/mnras/sts050](https://doi.org/10.1093/mnras/sts050)
- Gaspari, M., Ruszkowski, M., & Oh, S. P. 2013, MNRAS, 432, 3401, doi: [10.1093/mnras/stt692](https://doi.org/10.1093/mnras/stt692)
- Gaspari, M., Ruszkowski, M., & Sharma, P. 2012, ApJ, 746, 94, doi: [10.1088/0004-637X/746/1/94](https://doi.org/10.1088/0004-637X/746/1/94)
- Guo, F., & Mathews, W. G. 2014, ApJ, 780, 126, doi: [10.1088/0004-637X/780/2/126](https://doi.org/10.1088/0004-637X/780/2/126)
- Guo, F., & Oh, S. P. 2008, MNRAS, 384, 251, doi: [10.1111/j.1365-2966.2007.12692.x](https://doi.org/10.1111/j.1365-2966.2007.12692.x)
- Hardcastle, M. J., & Krause, M. G. H. 2013, MNRAS, 430, 174, doi: [10.1093/mnras/sts564](https://doi.org/10.1093/mnras/sts564)
- Heckman, T. M., Baum, S. A., van Breugel, W. J. M., & McCarthy, P. 1989, ApJ, 338, 48, doi: [10.1086/167181](https://doi.org/10.1086/167181)
- Hillel, S., & Soker, N. 2016, MNRAS, 455, 2139, doi: [10.1093/mnras/stv2483](https://doi.org/10.1093/mnras/stv2483)
- . 2017, MNRAS, 466, L39, doi: [10.1093/mnrasl/slz231](https://doi.org/10.1093/mnrasl/slz231)
- . 2020, ApJ, 896, 104, doi: [10.3847/1538-4357/ab9109](https://doi.org/10.3847/1538-4357/ab9109)
- Hogan, M. T., McNamara, B. R., Pulido, F., et al. 2017a, ApJ, 837, 51, doi: [10.3847/1538-4357/aa5f56](https://doi.org/10.3847/1538-4357/aa5f56)
- Hogan, M. T., McNamara, B. R., Pulido, F. A., et al. 2017b, ApJ, 851, 66, doi: [10.3847/1538-4357/aa9af3](https://doi.org/10.3847/1538-4357/aa9af3)
- Hudson, D. S., Mittal, R., Reiprich, T. H., et al. 2010, A&A, 513, A37, doi: [10.1051/0004-6361/200912377](https://doi.org/10.1051/0004-6361/200912377)
- Ikebe, Y., Makishima, K., Ezawa, H., et al. 1997, ApJ, 481, 660, doi: [10.1086/304095](https://doi.org/10.1086/304095)
- Imanishi, M., & Wada, K. 2004, ApJ, 617, 214, doi: [10.1086/425245](https://doi.org/10.1086/425245)
- Izumi, T., Kawakatu, N., & Kohno, K. 2016, ApJ, 827, 81, doi: [10.3847/0004-637X/827/1/81](https://doi.org/10.3847/0004-637X/827/1/81)
- Jacob, S., & Pfrommer, C. 2017, MNRAS, 467, 1449, doi: [10.1093/mnras/stx131](https://doi.org/10.1093/mnras/stx131)
- Kaasra, J. S., Ferrigno, C., Tamura, T., et al. 2001, A&A, 365, L99, doi: [10.1051/0004-6361:20000041](https://doi.org/10.1051/0004-6361:20000041)

- Kawakatu, N., & Wada, K. 2008, *ApJ*, 681, 73, doi: [10.1086/588574](https://doi.org/10.1086/588574)
- Kawakatu, N., Wada, K., & Ichikawa, K. 2020, *ApJ*, 889, 84, doi: [10.3847/1538-4357/ab5f60](https://doi.org/10.3847/1538-4357/ab5f60)
- Kitayama, T., Ueda, S., Akahori, T., et al. 2020, *PASJ*, 72, 33, doi: [10.1093/pasj/psaa009](https://doi.org/10.1093/pasj/psaa009)
- Kumar, P., & Johnson, J. L. 2010, *MNRAS*, 404, 2170, doi: [10.1111/j.1365-2966.2010.16437.x](https://doi.org/10.1111/j.1365-2966.2010.16437.x)
- Lacey, C. G., Baugh, C. M., Frenk, C. S., et al. 2016, *MNRAS*, 462, 3854, doi: [10.1093/mnras/stw1888](https://doi.org/10.1093/mnras/stw1888)
- Levin, Y. 2007, *MNRAS*, 374, 515, doi: [10.1111/j.1365-2966.2006.11155.x](https://doi.org/10.1111/j.1365-2966.2006.11155.x)
- Li, Y., Bryan, G. L., Ruszkowski, M., et al. 2015, *ApJ*, 811, 73, doi: [10.1088/0004-637X/811/2/73](https://doi.org/10.1088/0004-637X/811/2/73)
- Li, Y., Ruszkowski, M., & Bryan, G. L. 2017, *ApJ*, 847, 106, doi: [10.3847/1538-4357/aa88c1](https://doi.org/10.3847/1538-4357/aa88c1)
- Lim, J., Ao, Y., & Dinh-V-Trung. 2008, *ApJ*, 672, 252, doi: [10.1086/523664](https://doi.org/10.1086/523664)
- Loewenstein, M., Zweibel, E. G., & Begelman, M. C. 1991, *ApJ*, 377, 392, doi: [10.1086/170369](https://doi.org/10.1086/170369)
- Machida, M., Hayashi, M. R., & Matsumoto, R. 2000, *ApJL*, 532, L67, doi: [10.1086/312553](https://doi.org/10.1086/312553)
- Machida, M., & Matsumoto, R. 2003, *ApJ*, 585, 429, doi: [10.1086/346070](https://doi.org/10.1086/346070)
- Main, R. A., McNamara, B. R., Nulsen, P. E. J., Russell, H. R., & Vantyghem, A. N. 2017, *MNRAS*, 464, 4360, doi: [10.1093/mnras/stw2644](https://doi.org/10.1093/mnras/stw2644)
- Matsushita, K. 2001, *ApJ*, 547, 693, doi: [10.1086/318389](https://doi.org/10.1086/318389)
- Matsushita, K., Belsole, E., Finoguenov, A., & Böhringer, H. 2002, *A&A*, 386, 77, doi: [10.1051/0004-6361:20020087](https://doi.org/10.1051/0004-6361:20020087)
- McCourt, M., Sharma, P., Quataert, E., & Parrish, I. J. 2012, *MNRAS*, 419, 3319, doi: [10.1111/j.1365-2966.2011.19972.x](https://doi.org/10.1111/j.1365-2966.2011.19972.x)
- McDonald, M., Veilleux, S., Rupke, D. S. N., & Mushotzky, R. 2010, *ApJ*, 721, 1262, doi: [10.1088/0004-637X/721/2/1262](https://doi.org/10.1088/0004-637X/721/2/1262)
- McDonald, M., McNamara, B. R., van Weeren, R. J., et al. 2015, *ApJ*, 811, 111, doi: [10.1088/0004-637X/811/2/111](https://doi.org/10.1088/0004-637X/811/2/111)
- McDonald, M., McNamara, B. R., Voit, G. M., et al. 2019, *ApJ*, 885, 63, doi: [10.3847/1538-4357/ab464c](https://doi.org/10.3847/1538-4357/ab464c)
- McNamara, B. R., & Nulsen, P. E. J. 2007, *ARA&A*, 45, 117, doi: [10.1146/annurev.astro.45.051806.110625](https://doi.org/10.1146/annurev.astro.45.051806.110625)
- McNamara, B. R., Rohanizadegan, M., & Nulsen, P. E. J. 2011, *ApJ*, 727, 39, doi: [10.1088/0004-637X/727/1/39](https://doi.org/10.1088/0004-637X/727/1/39)
- McNamara, B. R., Russell, H. R., Nulsen, P. E. J., et al. 2016, *ApJ*, 830, 79, doi: [10.3847/0004-637X/830/2/79](https://doi.org/10.3847/0004-637X/830/2/79)
- . 2014, *ApJ*, 785, 44, doi: [10.1088/0004-637X/785/1/44](https://doi.org/10.1088/0004-637X/785/1/44)
- Meece, G. R., O’Shea, B. W., & Voit, G. M. 2015, *ApJ*, 808, 43, doi: [10.1088/0004-637X/808/1/43](https://doi.org/10.1088/0004-637X/808/1/43)
- Miki, Y., Mori, M., & Kawaguchi, T. 2021, *Nature Astronomy*, 5, 478, doi: [10.1038/s41550-020-01286-9](https://doi.org/10.1038/s41550-020-01286-9)
- Mittal, R., Hudson, D. S., Reiprich, T. H., & Clarke, T. 2009, *A&A*, 501, 835, doi: [10.1051/0004-6361/200810836](https://doi.org/10.1051/0004-6361/200810836)
- Mittal, R., McDonald, M., Whelan, J. T., & Bruzual, G. 2017, *MNRAS*, 465, 3143, doi: [10.1093/mnras/stw2915](https://doi.org/10.1093/mnras/stw2915)
- Nagai, H., & Kawakatu, N. 2021, *ApJL*, 914, L11, doi: [10.3847/2041-8213/ac03ba](https://doi.org/10.3847/2041-8213/ac03ba)
- Nagai, H., Onishi, K., Kawakatu, N., et al. 2019, *ApJ*, 883, 193, doi: [10.3847/1538-4357/ab3e6e](https://doi.org/10.3847/1538-4357/ab3e6e)
- Nagino, R., & Matsushita, K. 2009, *A&A*, 501, 157, doi: [10.1051/0004-6361/200810978](https://doi.org/10.1051/0004-6361/200810978)
- Navarro, J. F., Frenk, C. S., & White, S. D. M. 1997, *ApJ*, 490, 493, doi: [10.1086/304888](https://doi.org/10.1086/304888)
- Okabe, N., Umetsu, K., Tamura, T., et al. 2016, *MNRAS*, 456, 4475, doi: [10.1093/mnras/stv2916](https://doi.org/10.1093/mnras/stv2916)
- Olivares, V., Salome, P., Combes, F., et al. 2019, *A&A*, 631, A22, doi: [10.1051/0004-6361/201935350](https://doi.org/10.1051/0004-6361/201935350)
- Peterson, J. R., Paerels, F. B. S., Kaastra, J. S., et al. 2001, *A&A*, 365, L104, doi: [10.1051/0004-6361:20000021](https://doi.org/10.1051/0004-6361:20000021)
- Pfrommer, C. 2013, *ApJ*, 779, 10, doi: [10.1088/0004-637X/779/1/10](https://doi.org/10.1088/0004-637X/779/1/10)
- Pizzolato, F., & Soker, N. 2010, *MNRAS*, 408, 961, doi: [10.1111/j.1365-2966.2010.17156.x](https://doi.org/10.1111/j.1365-2966.2010.17156.x)
- Prasad, D., Sharma, P., & Babul, A. 2015, *ApJ*, 811, 108, doi: [10.1088/0004-637X/811/2/108](https://doi.org/10.1088/0004-637X/811/2/108)
- Pringle, J. E. 1981, *ARA&A*, 19, 137, doi: [10.1146/annurev.aa.19.090181.001033](https://doi.org/10.1146/annurev.aa.19.090181.001033)
- Pulido, F. A., McNamara, B. R., Edge, A. C., et al. 2018, *ApJ*, 853, 177, doi: [10.3847/1538-4357/aaa54b](https://doi.org/10.3847/1538-4357/aaa54b)
- Qiu, Y., Bogdanović, T., Li, Y., & McDonald, M. 2019a, *ApJL*, 872, L11, doi: [10.3847/2041-8213/ab0375](https://doi.org/10.3847/2041-8213/ab0375)
- Qiu, Y., Bogdanović, T., Li, Y., McDonald, M., & McNamara, B. R. 2020, *Nature Astronomy*, 4, 900, doi: [10.1038/s41550-020-1090-7](https://doi.org/10.1038/s41550-020-1090-7)
- Qiu, Y., Bogdanović, T., Li, Y., Park, K., & Wise, J. H. 2019b, *ApJ*, 877, 47, doi: [10.3847/1538-4357/ab18fd](https://doi.org/10.3847/1538-4357/ab18fd)
- Rafferty, D. A., McNamara, B. R., & Nulsen, P. E. J. 2008, *ApJ*, 687, 899, doi: [10.1086/591240](https://doi.org/10.1086/591240)
- Randall, S. W., Nulsen, P. E. J., Jones, C., et al. 2015, *ApJ*, 805, 112, doi: [10.1088/0004-637X/805/2/112](https://doi.org/10.1088/0004-637X/805/2/112)
- Romeo, A. B., & Falstad, N. 2013, *MNRAS*, 433, 1389, doi: [10.1093/mnras/stt809](https://doi.org/10.1093/mnras/stt809)
- Russell, H. R., McNamara, B. R., Edge, A. C., et al. 2014, *ApJ*, 784, 78, doi: [10.1088/0004-637X/784/1/78](https://doi.org/10.1088/0004-637X/784/1/78)
- Russell, H. R., McNamara, B. R., Fabian, A. C., et al. 2016, *MNRAS*, 458, 3134, doi: [10.1093/mnras/stw409](https://doi.org/10.1093/mnras/stw409)
- . 2019, *MNRAS*, 490, 3025, doi: [10.1093/mnras/stz2719](https://doi.org/10.1093/mnras/stz2719)
- Ruszkowski, M., Yang, H. Y. K., & Reynolds, C. S. 2017, *ApJ*, 844, 13, doi: [10.3847/1538-4357/aa79f8](https://doi.org/10.3847/1538-4357/aa79f8)

- Salomé, P., & Combes, F. 2003, *A&A*, 412, 657, doi: [10.1051/0004-6361:20031438](https://doi.org/10.1051/0004-6361:20031438)
- Salomé, P., Combes, F., Edge, A. C., et al. 2006, *A&A*, 454, 437, doi: [10.1051/0004-6361:20054745](https://doi.org/10.1051/0004-6361:20054745)
- Sanderson, A. J. R., Edge, A. C., & Smith, G. P. 2009, *MNRAS*, 398, 1698, doi: [10.1111/j.1365-2966.2009.15214.x](https://doi.org/10.1111/j.1365-2966.2009.15214.x)
- Sharma, P., McCourt, M., Quataert, E., & Parrish, I. J. 2012, *MNRAS*, 420, 3174, doi: [10.1111/j.1365-2966.2011.20246.x](https://doi.org/10.1111/j.1365-2966.2011.20246.x)
- Shlosman, I., Frank, J., & Begelman, M. C. 1989, *Nature*, 338, 45, doi: [10.1038/338045a0](https://doi.org/10.1038/338045a0)
- Simionescu, A., Tremblay, G., Werner, N., et al. 2018, *MNRAS*, 475, 3004, doi: [10.1093/mnras/sty047](https://doi.org/10.1093/mnras/sty047)
- Su, K.-Y., Hopkins, P. F., Hayward, C. C., et al. 2020, *MNRAS*, 491, 1190, doi: [10.1093/mnras/stz3011](https://doi.org/10.1093/mnras/stz3011)
- Sutherland, R. S., & Dopita, M. A. 1993, *ApJS*, 88, 253, doi: [10.1086/191823](https://doi.org/10.1086/191823)
- Tamura, T., Kaastra, J. S., Peterson, J. R., et al. 2001, *A&A*, 365, L87, doi: [10.1051/0004-6361:20000038](https://doi.org/10.1051/0004-6361:20000038)
- Thompson, T. A., Quataert, E., & Murray, N. 2005, *ApJ*, 630, 167, doi: [10.1086/431923](https://doi.org/10.1086/431923)
- Toomre, A. 1964, *ApJ*, 139, 1217, doi: [10.1086/147861](https://doi.org/10.1086/147861)
- Tremblay, G. R., O’Dea, C. P., Baum, S. A., et al. 2015, *MNRAS*, 451, 3768, doi: [10.1093/mnras/stv1151](https://doi.org/10.1093/mnras/stv1151)
- Tremblay, G. R., Oonk, J. B. R., Combes, F., et al. 2016, *Nature*, 534, 218, doi: [10.1038/nature17969](https://doi.org/10.1038/nature17969)
- Ueda, S., Ichinohe, Y., Molnar, S. M., Umetsu, K., & Kitayama, T. 2020, *ApJ*, 892, 100, doi: [10.3847/1538-4357/ab7bdc](https://doi.org/10.3847/1538-4357/ab7bdc)
- Ueda, S., Umetsu, K., Ng, F., et al. 2021, arXiv e-prints, arXiv:2106.07168. <https://arxiv.org/abs/2106.07168>
- Umemura, M., Fukue, J., & Mineshige, S. 1997, *ApJL*, 479, L97, doi: [10.1086/310592](https://doi.org/10.1086/310592)
- Vantyghe, A. N., McNamara, B. R., Russell, H. R., et al. 2016, *ApJ*, 832, 148, doi: [10.3847/0004-637X/832/2/148](https://doi.org/10.3847/0004-637X/832/2/148)
- Voit, G. M., & Donahue, M. 2015, *ApJL*, 799, L1, doi: [10.1088/2041-8205/799/1/L1](https://doi.org/10.1088/2041-8205/799/1/L1)
- Voit, G. M., Donahue, M., Bryan, G. L., & McDonald, M. 2015, *Nature*, 519, 203, doi: [10.1038/nature14167](https://doi.org/10.1038/nature14167)
- Voit, G. M., Meece, G., Li, Y., et al. 2017, *ApJ*, 845, 80, doi: [10.3847/1538-4357/aa7d04](https://doi.org/10.3847/1538-4357/aa7d04)
- Vollmer, B., Beckert, T., & Davies, R. I. 2008, *A&A*, 491, 441, doi: [10.1051/0004-6361:200810446](https://doi.org/10.1051/0004-6361:200810446)
- Wada, K., & Norman, C. A. 2002, *ApJL*, 566, L21, doi: [10.1086/339438](https://doi.org/10.1086/339438)
- Watabe, Y., Kawakatu, N., & Imanishi, M. 2008, *ApJ*, 677, 895, doi: [10.1086/528933](https://doi.org/10.1086/528933)
- Weinberger, R., Ehlert, K., Pfrommer, C., Pakmor, R., & Springel, V. 2017, *MNRAS*, 470, 4530, doi: [10.1093/mnras/stx1409](https://doi.org/10.1093/mnras/stx1409)
- Wilman, R. J., Edge, A. C., & Johnstone, R. M. 2005, *MNRAS*, 359, 755, doi: [10.1111/j.1365-2966.2005.08956.x](https://doi.org/10.1111/j.1365-2966.2005.08956.x)
- Wutschik, S., Schleicher, D. R. G., & Palmer, T. S. 2013, *A&A*, 560, A34, doi: [10.1051/0004-6361/201321895](https://doi.org/10.1051/0004-6361/201321895)
- Yao, Z., Yuan, F., & Ostriker, J. P. 2021, *MNRAS*, 501, 398, doi: [10.1093/mnras/staa3755](https://doi.org/10.1093/mnras/staa3755)
- Zweibel, E. G., Mirnov, V. V., Ruszkowski, M., et al. 2018, *ApJ*, 858, 5, doi: [10.3847/1538-4357/aab9ae](https://doi.org/10.3847/1538-4357/aab9ae)